UCRL-51421-74

X-Ray Emission from Laser-Produced Plasmas

C. E. Violet, Editor

July 1, 1974

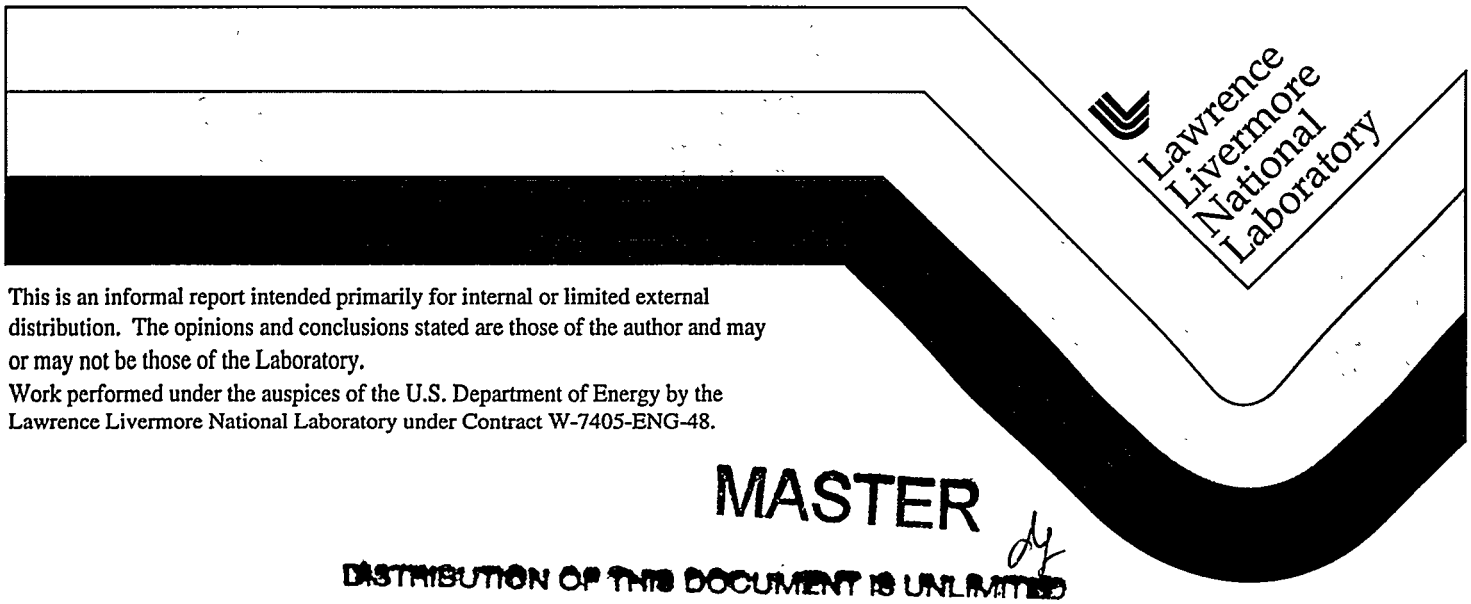

Work performed under the auspices of the U.S. Department of Energy by the Lawrence Livermore National Laboratory under Contract W-7405-ENG-48.

DISCLAIMER

Portions of this document may be illegible electronic image products. Images are produced from the best available original document.

93/435

X-RAY EMISSION FROM LASER-PRODUCED PLASMAS (U)

Annual Progress Report on Work Sponsored by the Defense Nuclear Agency

Period Covered: July 1973 through June 1974

C. E. Violet, Editor

July 1, 1974

AEC RESEARCH AND DEVELOPMENT
Prepared for U.S. Atomic Energy Commission under contract No. W-7405-Eng-48

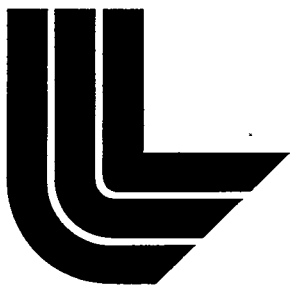

LAWRENCE
LIVERMORE
LABORATORY

University of California/Livermore

[redacted]

M-3679, C-74
Nuclear Weapons Related Engineering,
Instrumentation and Materials

This document contains 44 pages.

[redacted]

LAWRENCE LIVERMORE LABORATORY
University of California/Livermore, California/94550

[redacted]

UCRL-51421-74

X-RAY EMISSION FROM LASER-PRODUCED PLASMAS (U)

Annual Progress Report on Work Sponsored by the Defense Nuclear Agency

Period Covered: July 1973 through June 1974

C. E. Violet, Editor

MS. date: July 1, 1974

[redacted]

[redacted]

[redacted]

Foreword

This report summarizes computational and experimental activities carried out at Lawrence Livermore Laboratory in response to certain requirements of the Defense Nuclear Agency.

Subtask Code and Title: W99QAXPF001, Photon Source Research

Work Unit and Title: 16, Advanced Concepts

Source of funds supporting this research: IACRO 73-817

DNA Subtask Officer: Dr. Gordon K. Soper

[redacted]

[redacted]

Contents

[redacted]

X-RAY EMISSION FROM LASER-PRODUCED PLASMAS

Annual Progress Report on Work Sponsored by the Defense Nuclear Agency

Period Covered: July 1973 through June 1974

Abstract

The intensity and spectral characteristics of x rays emitted from laser-produced plasmas have been investigated computationally and experimentally. A two-dimensional implosion code was used successfully to calculate laser-plasma radiation characteristics and to aid in the design of laser targets for high-yield x-ray production. Other computer codes, in use or under development, predict line strengths and energies for laser-plasma x-ray emission. An experimental effort is aimed at reliable measurements of x-ray yields and spectra. A wide variety of x-ray detection methods have been evaluated, and x-ray yields have been measured from plasmas produced with two dissimilar laser systems. The high energy x-ray spectrum, from about 10 to 140 keV, has been studied using high-gain scintillation detectors and thick K-edge filters. Various supplementary measurements have provided information concerning characteristics of the target-reflected laser light, the ion energies, and the laser intensity patterns.

Introduction

The LLL DNA Laser program has the goal of developing an x-ray simulator capable of providing copious fluxes of x radiation. Since we intend to simulate blackbody radiators with temperatures of at least 1 keV, we are interested in achieving mean photon energies greater than 3 keV. For the test of small, isolated electronic components, modest fluxes of about 1 cal/cm^2 over several square centimeters will suffice. For full-scale tests of hardened reentry-vehicle components, the requirements are much more stringent — many calories per square centimeter over many square centimeters. To date, no experiment has satisfied these requirements. Mean photon energies for x rays from present experiments are well below 1 keV.

We are hopeful that the LLL laser program can meet these specifications. Code predictions indicate that with sufficient laser energy in a short enough pulse and with an appropriate target design we can attain these objectives. The lasers LLL is now building for the

[redacted]

fusion program are well suited to these goals; the first of these will be ready for use early in FY 1975, and the 10-kJ, subnanosecond laser will be ready in 1977. The dangers of basing programs on computer prognostications are well known, but we have gained some confidence in the reliability of the code by verifying that it properly calculates the results of present x-ray experiments. However, in these experiments the x radiation is predominantly emitted from relatively cool plasmas (energies of only several hundred electron volts).

Thus it is clear that we must continue to test our understanding of radiative processes. Experiments involving greater laser intensities, low-mass targets, and hotter plasmas are essential. The results of such experiments will provide the guidance for continued improvement of the design codes and modification of the target design. In addition to the laser construction program and target fabrication, LLL has a vigorous, diversified effort in the development of the diagnostic tools necessary for full interpretation of these experiments.

Computational Activities

LASER-PLASMA X-RAY COMPUTATIONS WITH LASNEX

Within the last year we have simulated several laser-plasma experiments with the two-dimensional Lagrangian hydrodynamics code LASNEX.[1] This hydrodynamics code is based on an average-ion model and assumes local thermodynamic equilibrium (LTE), but we are implementing a non-LTE version in which the average-ion level populations are computed by rate equations. The agreement between the LASNEX calculations and the experimental data reinforces our confidence in LASNEX.

Within the last year, LASNEX parameter studies have outlined the x-ray fluxes expected from the LLL 10-kJ Nd:glass laser. We have also used the code to design laser targets for the production of hard x rays. In addition, calculations have refined the plans for our experiments for the coming year. Finally, we have compared LASNEX calculations with the results of three types of experiments: x-ray micrographs, x-ray conversion efficiencies, and bremsstrahlung radiation from suprathermal electrons.

X-Ray Source Contours

We have developed an x-ray microscope (described more fully on p. 14) that uses grazing incident optics to attain higher sensitivity and higher resolution than would be possible with a pinhole. Figure 1 shows schematically the experimental arrangement of an x-ray micrograph taken at the 20-50 J, 3.5-nsec Long Path laser. The direction of observation is 45° to the normal to the target, which is a thick iron sheet. In the resulting micrograph, also shown in Fig. 1, the emission region appears as a flat disk viewed from the side. In the foreground one observes shadowing by cold ejecta thrown out of the crater. Since the measured resolution is better than 25 μm, the details seen in this micrograph (the

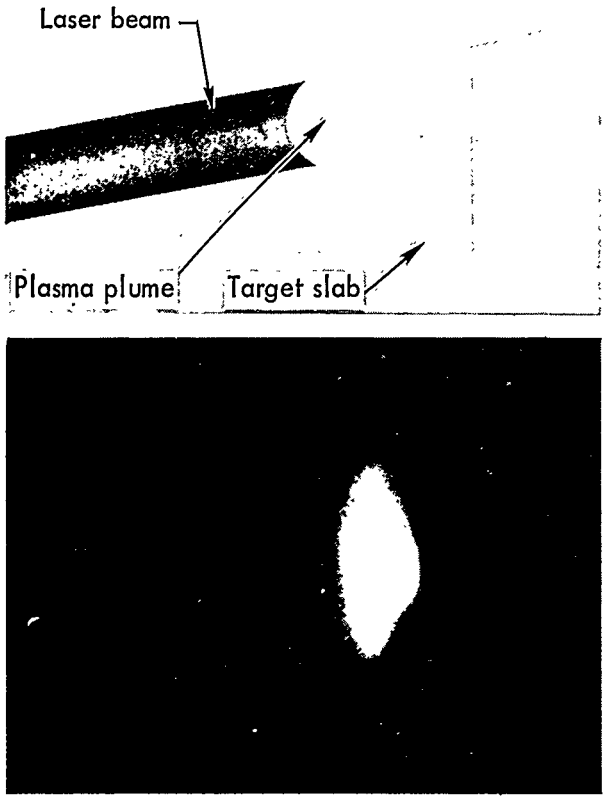

Fig. 1. Schematic representation of an experimental configuration in which a laser beam impinges on a flat iron slab, as viewed by an x-ray microscopy. The lower half of the figure shows the resulting micrograph.

spot diameter is several hundred micrometers) represent well-resolved features.

A post-processor code, TDG, has been written to predict the x-ray images associated with the plasmas simulated by LASNEX. Figure 2 illustrates the orientation of a solid of revolution, representing a plasma simulated by LASNEX, and the direction of the x-ray microscope, the observer. At prescribed times in its calculations, LASNEX writes a post-processor dump containing the position, electron temperature, density, and multigroup opacities of each Lagrangian zone. Subsequent to the LASNEX calculation, the code TDG reads each of these dumps and, by integrating the transport equation along rays parallel to the direction of observation, constructs the instantaneous x-ray image at any designated position and for any spectral range of x rays. The time-integrated image is formed from these.

The left image in Fig. 3 is a set of isoflux contours taken from an x-ray micrograph exposed at the 1-4 J, 100-300 psec Plasma-X laser. The target is an iron slab and the camera position is 45° to the normal from the target face. Only photons of at least 1.7 keV energy are imaged. On the right in Fig. 3 is the prediction of the LASNEX-TDG computation, which is in fair agreement with the data. LASNEX indicates that the x-ray emission is greatest for a narrow band between critical density and normal density and that thermal conductivity is so low that the heated area conforms almost exactly to the area illuminated by the laser — hence the disk-shaped emitting region.

X-Ray Conversion Efficiencies

With spot sizes deduced from x-ray micrographs, LASNEX calculations have predicted x-ray conversion efficiencies for experiments conduced on iron slabs at the Long Path and Plasma-X lasers. Table 1 compares the data and the calculations, along with the data and predictions for experiments conducted at the Battelle Memorial Institute.[2] Clearly, the LASNEX calculations reproduce the data rather well. Besides providing an opportunity to test LASNEX, these experiments have underscored the fact that in

(x',y',z'): Observation reference frame
(x,y,z): Coordinate system fixed by target

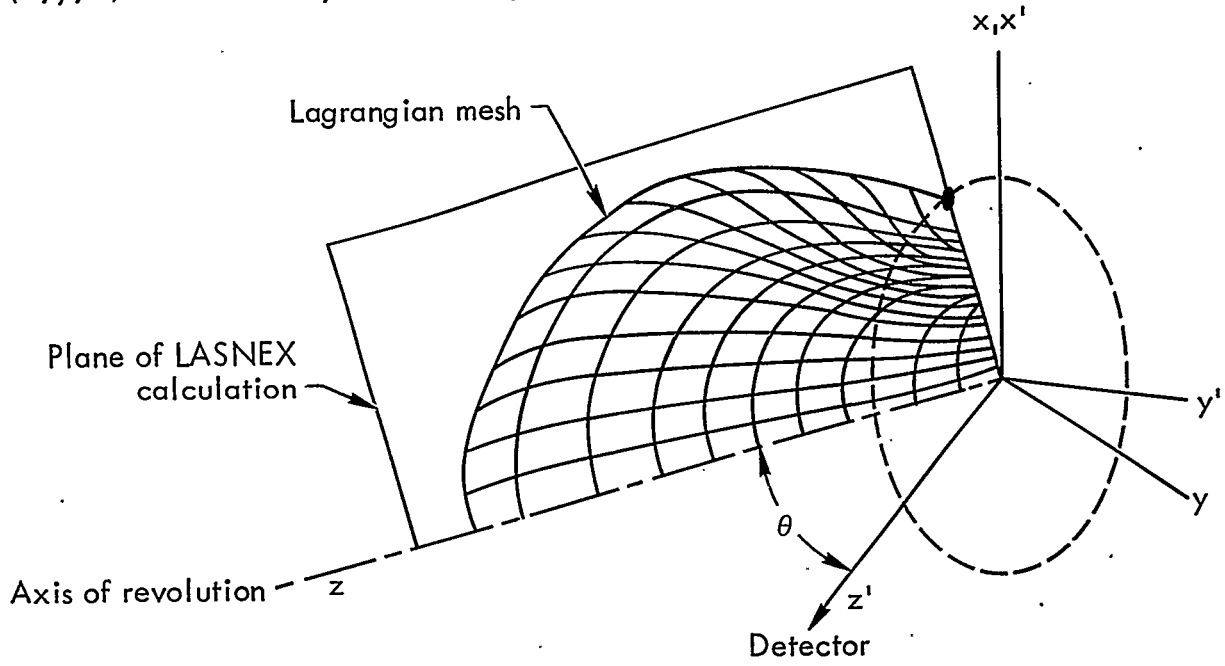

Fig. 2. Orientation of the plane of the LASNEX calculation and the direction of the x-ray microscope. The z axis is the axis of revolution for the calculation; the z' axis represents the direction of the x-ray microscope.

the laser irradiation of massive targets the resulting x rays are emitted principally by the relatively cool region (energy of a few hundred eV) between critical density and normal density and that this resulting x-ray spectrum is really too soft to be useful for simulating nuclear weapons effects. These experiments suggest then that future experiments must concentrate on low-mass targets.

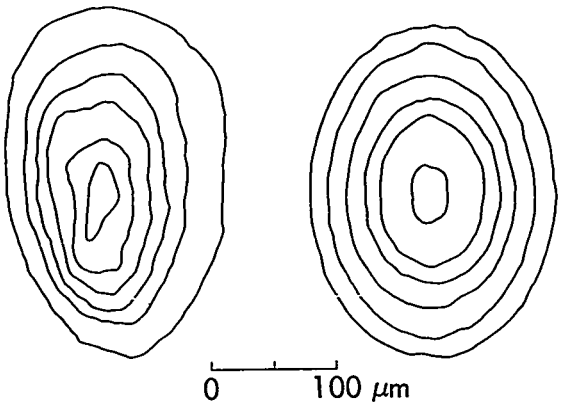

Fig. 3. Comparison of x-ray isoflux contours obtained from micrographs taken at the Plasma-X laser (left) with predictions of a LASNEX-TDG calculation (right).

Bremsstrahlung Radiation from Suprathermal Electrons

A series of experiments concluded recently at the Long Path laser suggest that the LASNEX calculations of plasma temperatures and density profiles are quite reliable. The first part of the experiment consisted in the absolute measurement of the x-ray spectra radiated by deuterated polyethylene (CD_2) slabs illuminated with the focused Long Path beam. These spectral data span the energy region from 0.5 to 150 keV and some 10 to 11 orders of magnitude in intensity. These measurements, obtained with several variations on the filter fluorescer

Table 1. X-ray yields (as percentages of laser-beam energy) from iron targets.

	Long Path laser (40 J, 3 nsec)	Plasma-X laser (1-2 J, 100-300 psec)	BMI laser (~40 J, 1.5 nsec)
Energies about 300 eV and higher:			
Measured	18%	18%	~27%
LASNEX calculation	11%	10-12%	~30%
Energies about 1.2 keV and higher:			
Measured	2%	1.5%	7-10%
LASNEX calculation	4%	1.5-5%	11-17%

technique, are described on page 10. Figure 4 shows the spectrum taken in one Long Path shot. For all energies, x-ray fluences obtained by detectors subtending given solid angles have been extrapolated to fluences expected over 4π. This assumption is valid for all but the softest photons (energies less than 2-3 keV), for which radiation is emitted over 2π because the CD_2 slab is thick to this radiation. For comparison with LASNEX calculations, which include the attenuation of photons traversing matter, one should reduce the dashed line by a factor as great as two for the softest x radiation. Figure 4 also depicts the results of LASNEX calculations; in one calculation ("below threshold") all the laser light is assumed to be absorbed by the process of inverse bremsstrahlung, while in the other ("above threshold") we assumed that all the light reaching 80% of critical density could be absorbed by anomalous processes as well. Absorption by inverse bremsstrahlung heats electrons to Maxwellian distributions, while anomalous absorption (by the excitation of a plasma instability) heats electrons in a distribution with high-energy tail — the suprathermal electrons, with a velocity distribution, $f(V) \propto \exp(-V^2/12V_{th}^2)$. LASNEX indicates that roughly 90% of the incident laser energy is absorbed by inverse bremsstrahlung before the light rays reach 80% of the critical density, the density at which the anomalous process

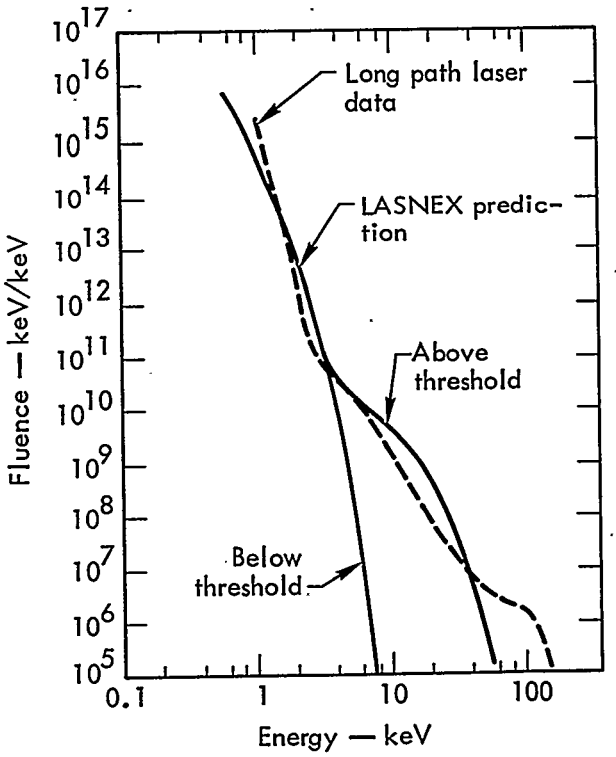

Fig. 4. Experimental and calculated x-ray spectral data.

becomes operative. The tail of hard x rays observed to photon energies of 150 keV is the signature of the suprathermal electrons. Had LASNEX predicted the density and temperature profile of the plasma blowoff incorrectly, then its estimate of the hard-x-ray spectrum would have been greatly in error, as illustrated by the curve generated exclusively by thermal radiation. That LASNEX can predict the spectrum over such an enormous dynamic range is impressive.

An additional series of experiments have determined the angular distribution of the hard x rays so that the angular distribution of suprathermal electrons can be ascertained. Calculations conducted with LASNEX and with a Monte Carlo electron-photon transport code, SANDYL, have also provided an interpretation of these data.

X-RAY TARGET DESIGN AND FABRICATION

As indicated in the previous annual report,[1] low-mass targets will be irradiated with the new Nd:glass lasers now being built. In light of the experimental evidence, low-heat-capacity targets appear essential to attain the high-temperature plasma required for the emission of intense x-ray fluxes (mean photon energies greater than 3 keV) suitable for weapon effects simulations. For the 50-J, 100-psec Janus laser facility (see p. 28) scheduled for experiments in mid-1974, the appropriate targets are "microdots" – thin (100-650 $\mu g/cm^2$) metallic (Al, Cu, Ag, or Au) disks 75-500 μm in diameter evaporated onto a very thin ($\geq$10 $\mu g/cm^2$) self-supporting foil. LASNEX calculations indicate that these targets will provide x-ray conversion efficiencies exceeding 50% with mean photon energies of 1 to 3 keV.

We are now perfecting the manufacturing process for these targets. We have fabricated masks for the prototype production of microdots of diameters 75, 150, 300, and 500 μm. The design of a "high-yield" mask for full-scale production is currently being completed. Evaporations of sample aluminum and gold microdots have been successfully conducted. The initial backing material under consideration had been carbon, but subsequent investigation indicates that considerable advantage in mass production process is obtained using instead a tough, thin (500 Å, ~5 $\mu g/cm^2$) plastic film. We have designed and built target holders compatible with the fixturing and positioning mechanisms in the 50-J target chamber.

LASER-PLASMA X-RAY COMPUTATIONS WITH FOREST-WAZER

Description of the FOREST-WAZER Program

The FOREST-WAZER computer program was developed to investigate the x-ray spectra of laser-heated plasmas in plane geometry. The FOREST program solves the time-dependent rate equations for the ionic populations of a multiple-ion, single-element gas without either LTE or average-ion assumptions. The program can handle up to 10 shells per ion and up to 12 ions per zone. FOREST also treats the emission of several thousands of lines, each being produced by an allowed transition of the valence electron between single excited configurations denoted

by the three quantum numbers n (principal), l (azimuthal), and j (total). The ions for a given zone form an ionic chain to which ions may be added (or subtracted from) as desired by the temporal changes of the zone. The WAZER program treats the deposition of laser light and determines the zonal temperature and density variations with time, which are given to FOREST for each WAZER time-step. FOREST supplies to WAZER at the start of each time-step a zonal sink term for the net emission rate of x rays from each zone.

In the FOREST program all line absorption is ignored except for the reduction of the initial line strength by multiplying by the probability of escaping the zone of origin. The latter is calculated by using a Doppler line profile characterized by the zonal temperature and by assuming that the line photon is emitted isotropically from the zone's center and is subject to absorption only by the line itself. Recently we have added continuous absorption to the program, with the result that radiative transfer for the continuum is solved exactly, assuming no time retardation. All photons, including the "reduced" line photons, are assumed to be emitted uniformly throughout each zone.

FOREST has also been generalized to handle a mixture of a single element with bound electrons and up to ten elements that are assumed to be completely stripped of bound electrons for the duration of the problem.

Computational Results

In the development of the FOREST-WAZER computer program we have solved three test problems involving a zirconium slab (Z = 40). The first two calculations were made without continuous absorption, and each required more than two hours of CDC-7600 running time. The third problem included continuous absorption, but due to improvements in the efficiency of the FOREST program it required less than one hour to run.

For the first problem we assumed a trapezoidal-shaped pulse of laser light of wavelength 1.06 μ and total energy 7500 J/cm^2 with a full width at half maximum of 75 psec; the problem was run for 300 psec. This problem was the same as an earlier problem calculated by MONTE-WAZER that used a cruder ion model (called the average-ion model).[1] The overall calculated x-ray emission was similar above 1 keV but much less in the FOREST calculation for x rays below 1 keV. However, MONTE-WAZER had continuous absorption, thus accounting for the difference.

The second calculation used a profile whose total energy was the same as in the first calculation but whose pulse width was twice as long. The problem was run for 500 psec. The x-ray spectra was essentially unchanged.

The third calculation was the same as the second but included continuous absorption. Several small errors present in the previous calculations were discovered and eliminated. The results show a front-surface to rear-surface emission ratio of two, which is comparable with the factor of 2.5 determined by the MONTE-WAZER problem. The line spectrum from the front surface is not modified significantly by continuous absorption, but the continuous emission is increased by a factor of 3.5.

The systematic computation of x-ray efficiencies and spectra for different-Z targets, with various laser light profiles, is in progress.

Experimental Activities

Our investigations of laser-produced plasmas continue to be guided by the need for an understanding of laser-target interaction mechanisms and of those plasma characteristics, such as anomalous electron distributions, that are especially significant for laser fusion. We have enhanced our ability to explore spectral and geometrical features of laser-produced plasmas with the completion of two new instruments. One of these – a simple x-ray microscope – has been used to examine the spatial characteristics of the x-ray-emitting plasmas produced with our laser systems. The LASNEX computer program has successfully reproduced characteristic features of the micrographs obtained with the x-ray microscope. A second instrument has resulted from our ability to bend potassium acid phosphate (KAP) crystals to a small radius of curvature, leading to an x-ray spectrograph that permits the examination of a broad spectral range with a single exposure. The spectral data are converted to absolute values with the aid of a computer program.

Our studies of the very high energy x rays (above about 10 keV) emitted from laser-produced plasmas have been augmented by simultaneous measurements of the low-energy spectrum and by investigations of the angular distribution of the high-energy x rays. These experiments, in conjunction with the corresponding computational studies, are providing information on laser-plasma coupling mechanisms of special significance for laser fusion. Since a knowledge of the intensity of focused laser beams is essential to the study of laser-target interactions, we have developed an experimental and computational technique that provides detailed information concerning the intensity pattern of the focused beam. Other developments include improvements in the accuracy with which we measure the x-ray yield from laser-produced plasmas and, consequently, an increased knowledge of the efficiency with which laser light is converted to soft x rays by plasma production. We have also developed a new method of measuring the total laser light reflected from the target and have obtained some preliminary results. Many of these diagnostic techniques are increasingly used in parallel, which provides data that are particularly helpful in constructing a more complete picture of laser-plasma characteristics.

LASER FACILITIES

The Long Path and Plasma-X lasers[1] continued to operate as facilities for laser-plasma interaction experiments and diagnostic development. The following experimental work using planar targets was carried out during the past year:

- Long Path laser
  1) Spectral distribution of x rays from a plasma produced by the laser;

2) X-ray conversion efficiency;

3) Laser light reflection from laser produced plasmas (backward hemisphere).

For these experiments the laser delivered about 1250 pulses at energies between 20 and 50 J in about 3.5 nsec.

- Plasma-X laser

  1) X-ray conversion efficiencies;

  2) Diagnostic development of the x-ray microscope (see p. 14), the x-ray streaking camera (see p. 21), and MOSFET x-ray detectors (see p. 10);

  3) Back-reflected laser light (through focusing lens) measurements.

For these experiments the Plasma-X laser was pulsed about 1300 times. The laser delivered pulses between 1 and 4 J in 100 to 300 psec. The Plasma-X laser was dismantled in December 1973.

Table 2. Experimental laser-light-to-x-ray conversion efficiences (average efficiencies for isotropic emission in 2π steradians).

Target	Absorber	Efficiency (%)[a]
Plasma-X laser (1-5 J in ~300 psec):		
CH_2	$\frac{1}{2}$-mil Be	0.005
C	$\frac{1}{2}$-mil Be	0.02
Al	$\frac{1}{2}$-mil Be	0.27
Zr	$\frac{1}{2}$-mil Be	0.35
Ta	$\frac{1}{2}$-mil Be	0.60
Pb	$\frac{1}{2}$-mil Be	0.35
Fe	1850-Å Al	18
Fe	$\frac{1}{2}$-mil Be	1.5
Fe	1-mil Be	0.30
Long Path laser (20-50 J in ~3 nsec):		
Fe	1850-Å Al	18
Fe	1/3-mil Be	3
Fe	$\frac{1}{2}$-mil Be	2
Fe	5.33-mil Be	0.05

[a]The accuracy of the measurement made with the thin aluminum absorber is about 50%; the accuracy of the other measurements is about 25%.

X-RAY CONVERSION EFFICIENCY

Efforts have continued to develop and evaluate x-ray calorimeters and improve the accuracy of measurements of x-ray fluence and laser-light-to-x-ray conversion efficiencies. Among the detectors we have tested extensively are two that are well suited to laser-plasma x-ray yield measurements and appear to provide very reliable results. These detectors — the silicon surface barrier (SiSB) detector and a special thin-film thermopile matrix (TPM) detector — give absolute energy readings that are in excellent agreement (±10%) when used simultaneously to measure laser-plasma x-ray yields. We conclude that we are now able to measure x-ray fluences from laser-produced plasmas to an accuracy of ±10%. The TPM seems particularly appropriate for the higher x-ray fluences anticipated in future experiments with higher-energy lasers. Both detectors require some special care under certain circumstances; the performance of the SiSB detector may be degraded by exposure to excessively high x-ray fluxes, and careful shielding from electrical noise is an important requirement for satisfactory operation of the TPM.

Table 2 gives our most recent determinations of the laser-light-to-x-ray conversion efficiences obtained using the Plasma-X and Long Path lasers. The conversion efficiency is the percentage of

the incident laser energy that is reemitted as x rays from the target plasma into the backward 2π steradians and transmitted by a specified absorber. The measurements were made at an azimuthal angle of 135° from the laser beam direction. The conversion efficiency is determined from the measurements on the assumption of isotropic x-ray emission into the backward hemisphere. Fluctuations in the efficiency for these lasers is about ±50%. The accuracy of the average value of the efficiency is about 50% for the thinnest absorber (1850-Å Al) and 25% for the thicker absorbers. The errors involved in these efficiency measurements include errors in measuring the incident laser light and in determining the x-ray transmission losses in the imperfectly evacuated target chamber. Interestingly, the average conversion efficiencies for the iron target and both the 1850-Å aluminum and the $\frac{1}{2}$-mil beryllium absorbers are, perhaps fortuitously, about the same for both lasers. Also, the measured conversion efficiencies obtained with the Plasma-X laser show a variation with Z that is consistent with similar measurements reported by NRL[3] and Lockheed.[4]

HIGH-ENERGY X-RAY SPECTRUM

The high-energy (above about 10 keV) x-ray spectrum from laser-produced plasmas is of special interest because of its relationship to plasma instabilities excited by the intense laser light. High-energy x rays may therefore provide an important key to the understanding of the physics of laser-plasma coupling mechanisms. Of particular interest is the fact that instability heating may produce a suprathermal electron spectrum, which is potentially detrimental for some laser fusion schemes.

Table 3. Detector channels for 1-50 keV x-ray spectra measurements.

Energy (keV)	Filter	Detector
1	Be	MOSFET
1.5	Al	MOSFET
3	Cl	MOSFET
3	Cl	0.13-mm plastic scintillator
5	Ti	0.13-mm plastic scintillator
9	Zn	0.26-mm plastic scintillator
25	Sn	NaI(Tl)
50	Er	NaI(Tl)

The x-ray spectrum for a laser-heated CD_2 target from about 10 keV to about 100 keV has been determined with improved accuracy.[5] The improvement resulted in part from auxiliary measurements in which we obtained the x-ray angular distribution as a function of x-ray energy.

We have performed spectrum measurements between 1 and 50 keV using the K-edge filter technique; Table 3 shows the filters and detectors and nominal energies used to make the measurements. Calibrations of the fluor-photomultipliers for x rays below 8 keV were done at the LLL x-ray facility at EG&G, Las Vegas. The metal-oxide semiconductor/field-effect transducer (MOSFET) detectors were calibrated at 6.40 and 8.05 keV – two energies were necessary to infer a SiO_2 thickness from the calibrations. With a known thickness the detector response can be calculated with confidence at the lower x-ray energies. With these

calibrations accomplished, we carried out a final analysis of the data.

The final analysis revealed an x-ray spectrum (dashed curve of Fig. 4) that falls rapidly with increasing x-ray energy up to about 3 keV. This portion of the curve is thought to be the thermal x-ray spectrum. At about 3 keV there is a drastic change in the slope of the curve corresponding to the onset of the suprathermal tail. As far as we know this is the first simultaneous measurement ever made of the thermal and nonthermal x-ray spectrum from a laser-produced plasma. No data was taken for x-ray energies greater than 50 keV, but from previous measurements it is known that the spectrum levels off and is almost flat up to about 100 keV. Folded into these results is the fact that the high-energy x rays (above 25 keV) are emitted anisotropically with a fore-aft ratio of about 3:1 (see Fig. 5).

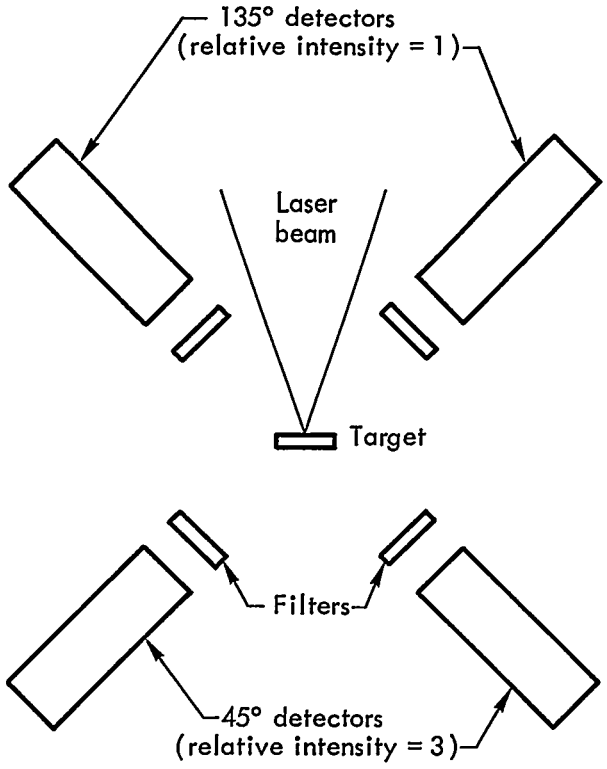

Fig. 5. Relative intensity of x-ray signals at 45° and 135° from the direction of a laser beam striking a target.

To compare the measurements with calculations, we took far-field pictures of the laser beam to determine the profile of the focused laser beam. The beam contour for the laser shot that produced the x-ray spectrum shown in Fig. 4 is shown in Fig. 6. The peak intensity was 1.6×10^{13} W/cm^2. The graph at the right shows the data in reduced form for use in the calculational codes; note that only about 1% of the total beam profile is at the maximum beam intensity, while most of the area is at about 20% of the peak intensity.

LASNEX was used to calculate the high-energy tail of the x-ray spectrum. Since the measurements were extended down to the thermal energy region, the thermal temperature is no longer a free parameter in the calculations. Figure 4 shows the results of two LASNEX calculations using the beam profile in Fig. 6; one calculation assumed only absorption by inverse bremsstrahlung, the other allowed only a fraction of the laser light reaching the critical density to produce suprathermal electron velocity distributions. Clearly, inverse bremsstrahlung alone does not describe the experimental results very well. However, inclusion of the suprathermal electron distribution produced an x-ray spectrum that reasonably fits the bulk of the high-energy x rays up to about 50 keV. The high-energy plateau region from 50 to 100 keV was not calculated.

To determine if the x-ray intensity is correlated with the total laser energy delivered to the target, we did a

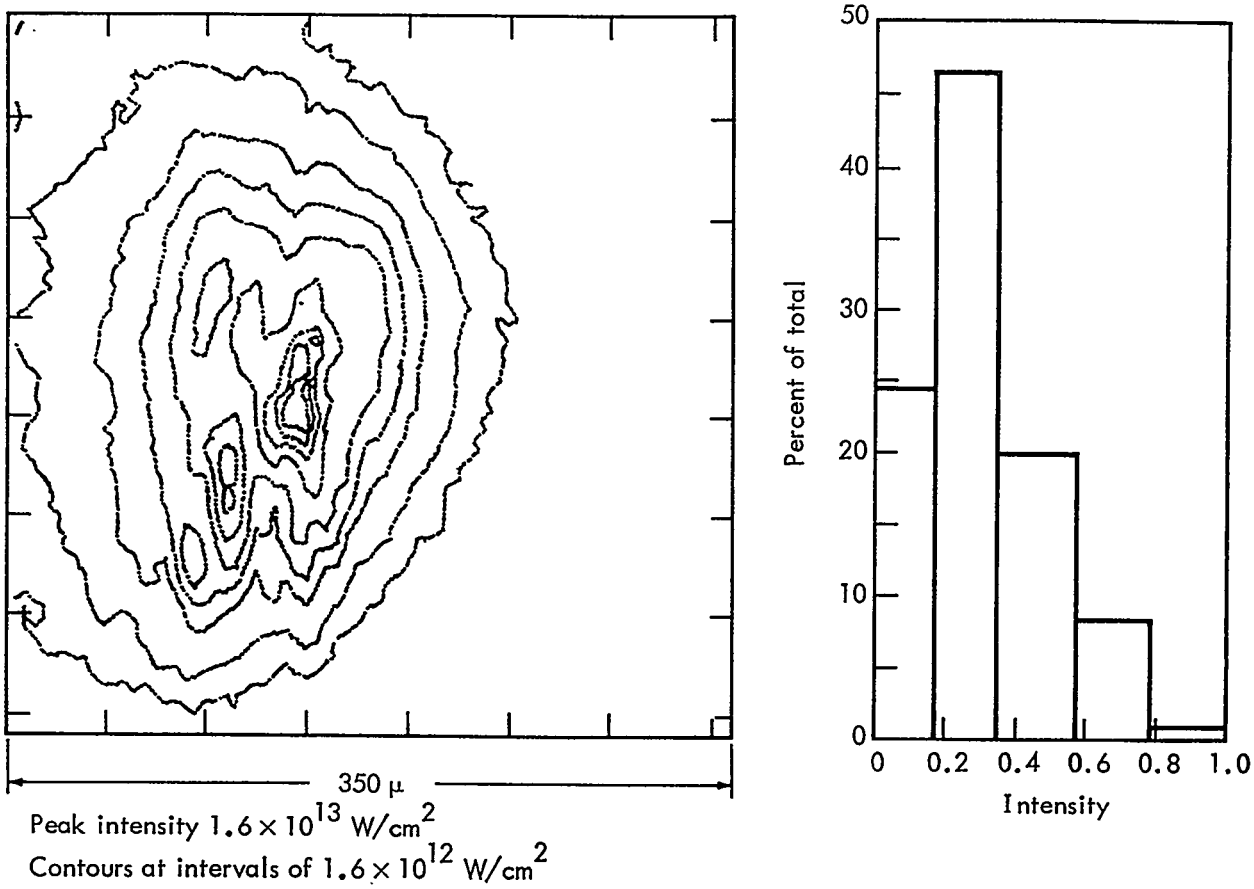

Fig. 6. Far-field beam-contour image for the laser shot that produced the x-ray spectrum in Fig. 4. The peak intensity was 1.6×10^{13} W/cm^2; the contour interval is 1.6×10^{12} W/cm^2.

statistical analysis of 14 laser shots. The results showed that for x rays in the thermal portion of the spectrum there was a high correlation between the energy delivered to the target and the measured x-ray intensity. As the target energy increased, the x-ray output increased. But for measurements made in the suprathermal tail, we could find no correlation. However, from the only three laser shots that were analyzed in detail there appears to be a correlation between the suprathermal x-ray intensity and the laser beam intensity (not energy). Further analysis of other laser shots will be carried out to verify this tentative conclusion.

We also carried out a detailed analysis of the multiple-target experimental results (reported on p. 10) involving measuring the anistropy of the high-energy x-ray emission from CD_2, tantalum, and CD_2-Ta targets. The purpose of these experiments was to gain more information on the electrons that produce the x rays in the plateau region from 50 to 100 keV. We found that the emission of 80-keV x rays from the CD_2 target is anisotropic. However, the same emission from a thin tantalum target is almost isotropic. The reason for this is that the fast electrons that are formed in the plasma suffer large-angle scattering due to elastic collisions with high-Z nuclei before they lose their energy in

small-angle collisions with atomic electrons. In an attempt to determine the approximate electron energy, we used a target of 0.25 mm CD_2 backed with 0.05 mm tantalum. The fore-aft asymmetry of the 80-keV x rays was 0.6:1. The interpretation of this result is that the laser light is absorbed in the CD_2 and high-energy electrons are produced. These electrons are energetic enough to traverse the thin CD_2 and still have enough energy left over to produce 80-keV x rays in the tantalum. X-ray absorption in the tantalum prevents the fore-aft ratio from being 1:1. We also used another target with thicker CD_2: 1.02 mm CD_2 backed with 0.05 mm tantalum. The fore-aft measurement with this target was almost identical to that of just CD_2, indicating that the electrons in this case are not energetic enough to get through the thicker CD_2. Detailed analysis of the x-ray distribution from the composite targets and others indicates that the mean energy of the electrons responsible for the "plateau" x rays is about 300 keV and that they enter the cold target material in a cone whose half angle is approximately 45°. Thus there appears to be a dominant forward component (in the direction of the laser propagation) of the electrons in the cold material.

Future plans (see p. 34) include developing accurate, reliable, compact instruments for measuring absolute x-ray spectra from 400 eV to 100 keV. These will provide the x-ray diagnostics for analyzing the sophisticated targets we are now designing. We are also developing high-resolution instrumentation for measuring broadening of Kα lines, from which information on ion density may be inferred.

X-RAY SPECTROSCOPY

We have augmented our spectroscopic capabilities with the development of a bent KAP crystal spectrograph. The crystals are bent to a radius of only 2 to 3 cm, thereby providing a broad range of spectral coverage from approximately 600 eV to 10 keV. We have used the new spectrograph to examine the x-ray emission from various targets irradiated with the Long Path laser. Interpretation of these spectra is currently in progress.

X-RAY MICROSCOPY

We have built a simple microscope to study the properties of this type of instrument and to take data concerning laser-generated plasmas. Using this information we have developed a more complicated microscope that we are just starting to use on-line as a data collecting device. Computer design studies are also underway to develop more elaborate systems for future needs.

Single-Lens Microscope

At grazing incidence, x rays can be almost totally reflected from smooth surfaces. We have used this phenomenon to build a simple x-ray lens (see Fig. 7). The reflection process is such that, for a given material, soft x rays are reflected with high efficiency but as photon energy is increased the reflection efficiency drops rapidly until a "cutoff" energy is reached. At energies higher than this

there is no reflection. This cutoff can be quite sharp and is thus useful in making spectral measurements.

The potential advantages of an x-ray microscope to laser diagnostics are: (1) spatial resolution is good – 10 μm is easy to achieve with a simple system (Fig. 8); (2) the lens can be placed far from the target, keeping this region free for other diagnostics; and (3) the high-energy cutoff makes absolute measurement of soft x-ray fluxes easier.

Our single-lens system consists of two glass surfaces. Each surface is ground and polished to a slightly concave cylinder. The radius of curvature, R, is about 1000 in. Each element acts as a cylindrical lens for x rays incident on the surface at an angle, i, of less than 1°. The focal length of each element is given by f = R sin (i/2), and each element takes rays from a point source to a line focus. The two elements are oriented so that a small fraction of the source x rays are reflected from both surfaces. The reflection planes are perpendicular, so the combination of the two line foci is a true image of the source.

Our single lens has a glass reflection surface with an angle of incidence of 0.8° and a focal length of 10.5 in. The system is set up to operate with a magnification of about 3. The lens is 14 in. from the laser target and the image is recorded on film 42° behind the lens. The lens uses only a small fraction of the x rays. The effective solid angle subtended at the target is 6×10^{-8} steradians.

Using the Plasma-X and Long Path lasers and a variety of targets we have investigated the properties of this single-lens system. Our important findings

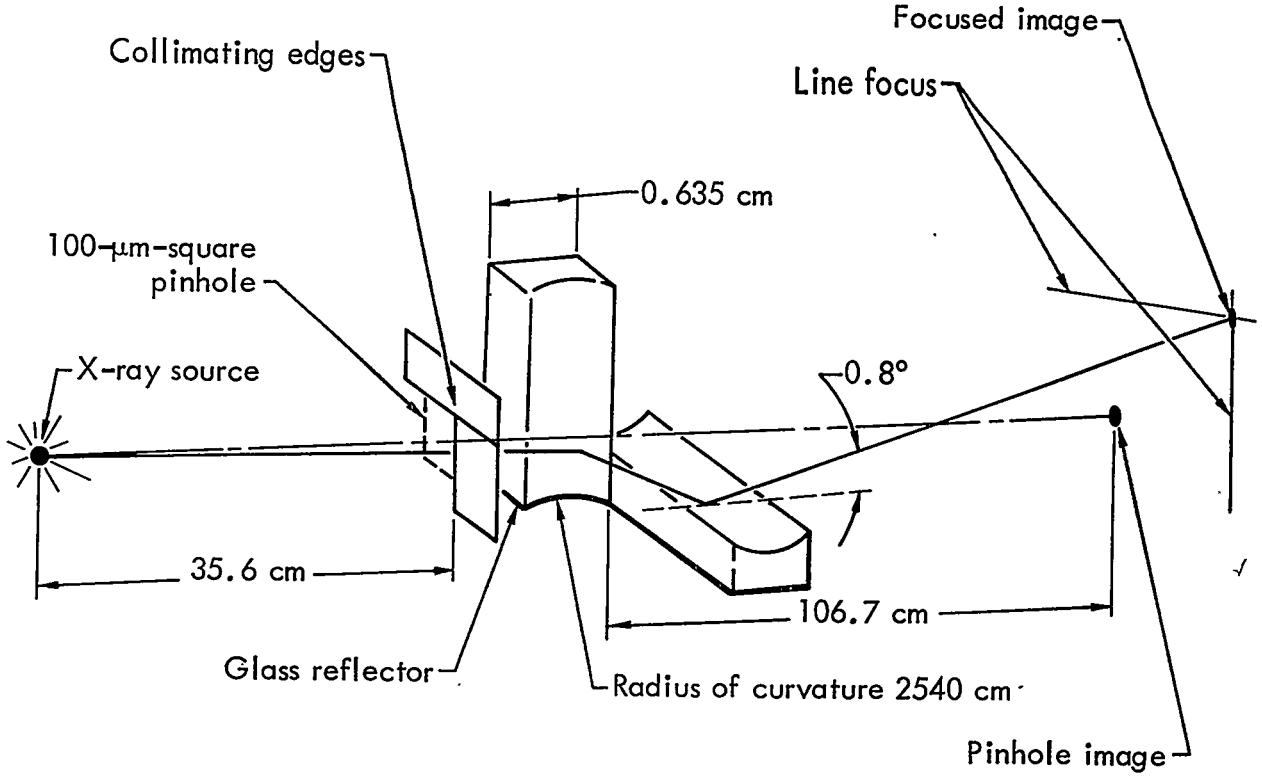

Fig. 7. Schematic representation of the x-ray microscope used to study laser-produced plasmas.

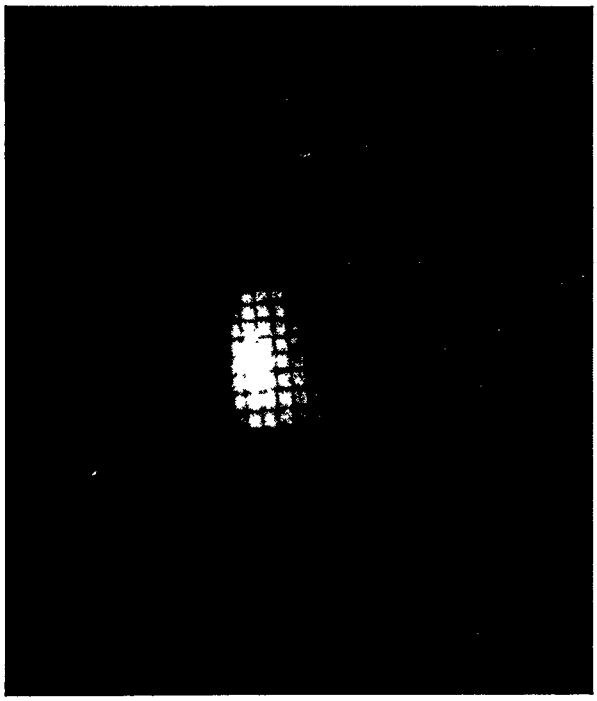

Fig. 8. X rays generated by the Long Path laser viewed by the single-lens microscope through a 1000 line-per-inch mesh. The sharpness of the image implies a resolution of about 5 μm. The laser target was an iron slab; the laser energy was about 20 J.

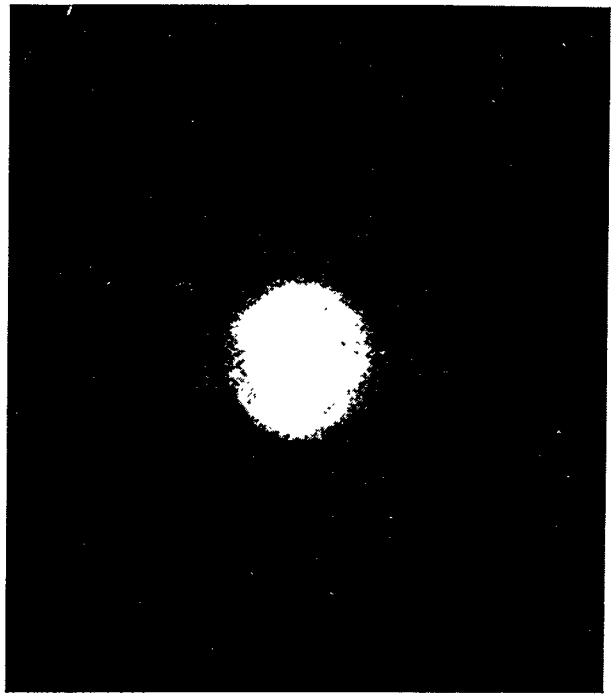

Fig. 9. Single-lens-microscope picture of the x rays from a glass shell target. The glass sphere had a radius of 100 μm and a wall thickness small by comparison. The microscope view angle was 135° from that of the incident laser light.

are as follows. (1) The system is sensitive enough that film can be used to record the image for most targets (Fig. 9). This is much simpler than active electronic recording devices and makes precise flux measurements possible. (2) Focal conditions are not critical. The two mirrors do not have to be positioned with extreme precision for optimum operation. This makes setup and operation easy. (3) The resolution of the lens is better than expected. Details 5 to 10 μm in size can be seen over a field of view of several hundred micrometers.

If the absolute calibration of the system is known, the pictures obtained can be used to derive the absolute spectral energy flux from different regions of the plasma. Towards this end we have calibrated the sensitivity of three types of film to 900-eV x rays. We are working towards extending this calibration to other energies spanning the soft x-ray region in which the microscope operates.

Pinhole Camera

To complement the x-ray microscope we have constructed a simple pinhole camera. An array of 16 pinholes, ranging in diameter from 6 to 75 μm, in a 1-mil gold foil, produces simultaneous pictures at different sensitivities and resolutions. Several filters are also used to eliminate varying amounts of soft x rays.

The advantages of the pinhole camera are that it records high-energy x rays (there is no energy cutoff as in the microscope, so photons of all energies can be recorded) and that it can be used to record faint, diffuse features of the x-ray-emitting regions. By use of a large pinhole, the camera sensitivity can be increased greatly with a consequent loss of resolution (see Fig. 10). There are applications in which this is desirable.

Our plan is to use the pinhole camera and x-ray microscope simultaneously. Different phenomena are recorded by the two instruments, and the region of overlap can be used to check sensitivity calculations.

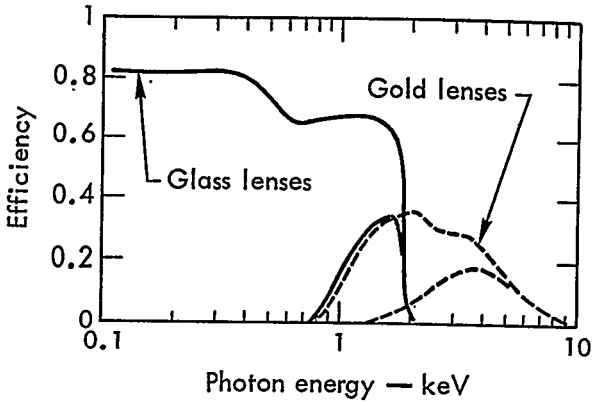

Fig. 11. Calculated efficiency of the four-lens microscope. The efficiency is a function of the reflection efficiency of the glass and gold lenses and the properties of the filters used. Different filters can easily be substituted to change the relative sensitivities.

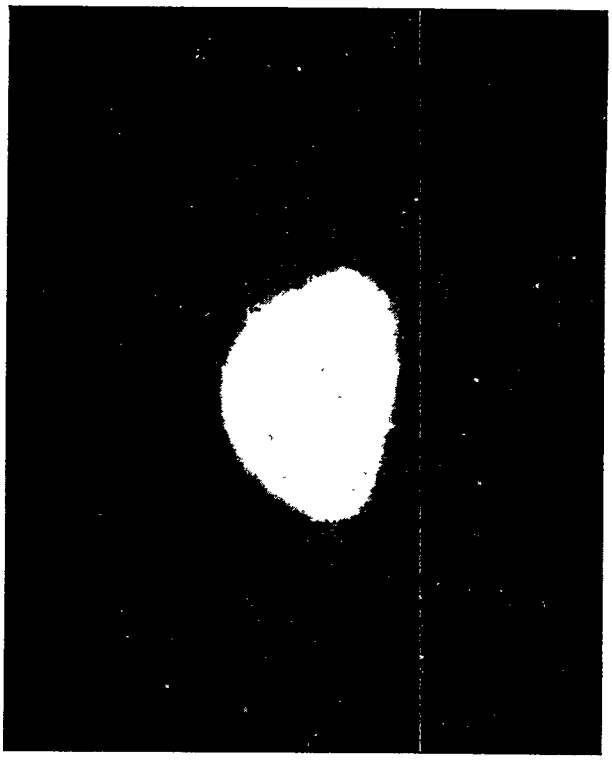

Fig. 10. Pinhole camera picture of the x rays from the same glass shell target as in Fig. 9. The pinhole diameter was 12 μm. Note both the x rays from the glass shell and the faint emis- from the surrounding region.

Four-Lens Microscope

Using the measured focal properties of the single-lens system, we have designed and built a four-lens microscope. This takes four pictures at the same time and will be used to record spatial x-ray emission in four different energy ranges. Two lenses are glass reflectors and two lenses are gold reflectors; the energy cutoff for reflection from a gold surface is higher than that from glass. The gold lenses are expected to produce images at higher energies (Fig. 11).

This four-lens microscope has been set up at the Long Path laser. We have found that the mechanical tolerances for the lens mounting are much more severe than those of the single-lens system. After making a mechanically exact lens holder and grinding the lenses to higher tolerances, we have taken pictures showing that all four lens are focused and have resolutions better than 10 μm. Work

is under way to study several targets using this four-lens system.

High-Sensitivity Microscope Lens

We are designing a large-area lens. A figure of revolution with cylindrical symmetry can be designed that will intercept a larger fraction of incident x rays and bring them to a focus. We are modifying a ray-tracing program for use on our computers. This program will be used to find the optimum shape for this lens. We expect this lens to be 1000 times as sensitive as the single-lens microscope we now have. The new lens might be used with filters that pass only a narrow band of energies to take pictures using one particular emission line. An objective grating spectrograph is another possible application.

RELATED PLASMA MEASUREMENTS

Laser-Light Target-Reflection Measurements

A knowledge of the intensity and directional characteristics of the laser light reflected from the target is an essential ingredient in the study of laser-target interactions. We have developed a new technique that permits a determination of the total laser light reflected from the target during plasma production. The method can also be used to provide a photographic record of the spatial intensity pattern of the reflected laser light. The central feature of the method is the use of a parabolic reflector located so as to collect the target-reflected light and direct it through a window at the rear of the target chamber, as shown in Fig. 12.

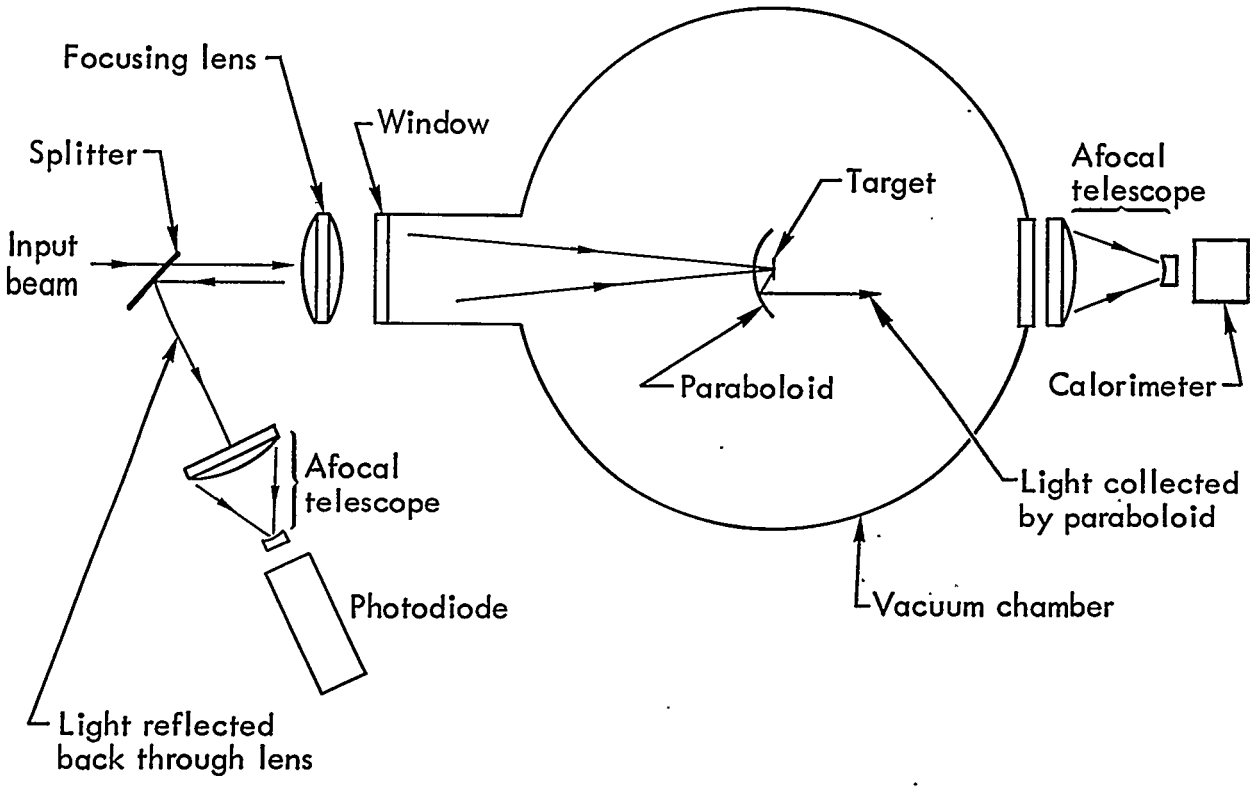

Fig. 12. Principal components of the target-reflection experiments done with the Long Path laser system.

The light is then photographed or focused into a calorimeter. The incident laser light reaches the target by passing through a hole in the center of the parabolic reflector. The light reflected back through this hole passes through the focusing lens and is monitored with the aid of a beam splitter. Preliminary results using an f/7 focusing lens with the Long Path laser system and a CH_2 target indicate a total reflection equal to less than 10% of the incident laser light. Additional measurements with improved reflectors are in progress.

We have also made measurements of the back-reflected laser light from a variety of planar targets with the Plasma-X laser using an f/3 focusing lens. For all the targets used – CH_2, C, Al, Fe, Zr, and Ta – the back-reflected light was 4 ± 2%.

Laser Beam Intensity Profiles

A determination of the far-field pattern of a laser's output beam can provide information concerning the intensity profile of the focused beam at the target. Such data is of key importance in any attempt to analyze laser-target interactions. The method we have developed for far-field exploration involves the calorimetric determination of total laser energy, photodiode measurement of laser intensity as a function of time, and densitometer measurements of multiple-image far-field patterns.

Figure 13 shows schematically the optical systems used for beam analysis

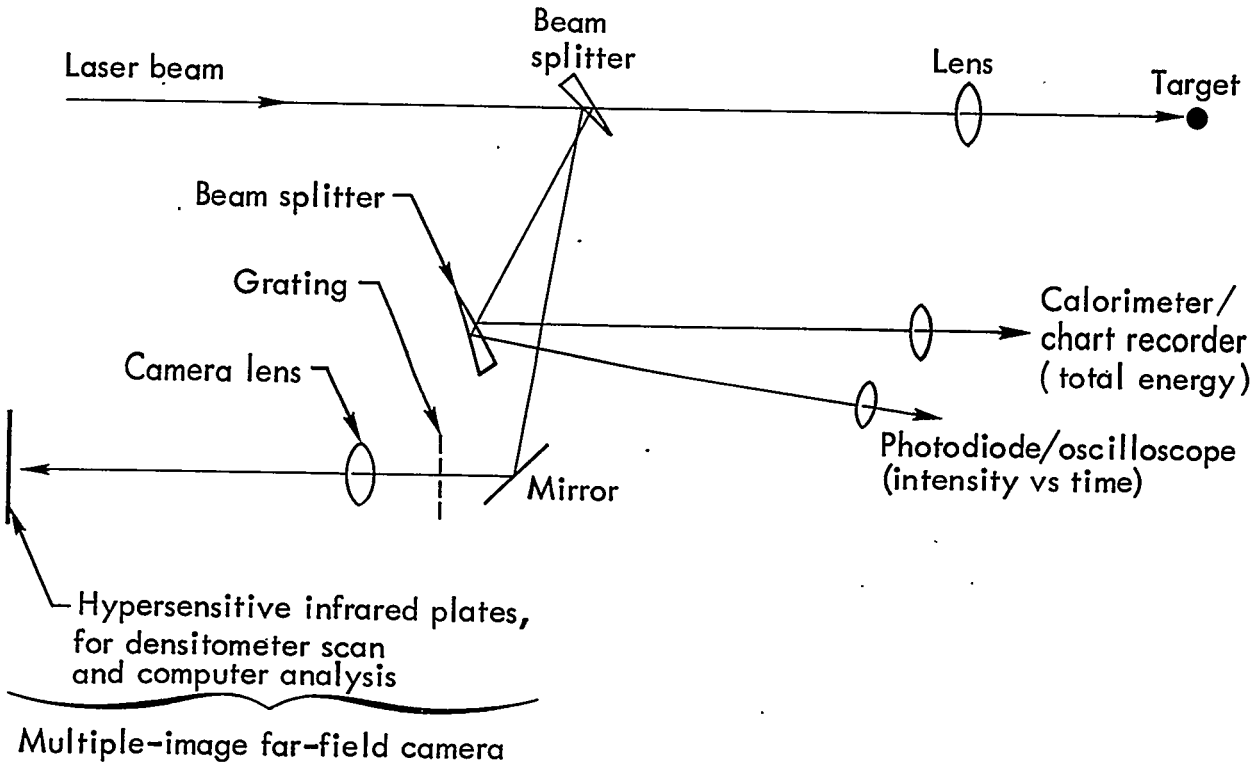

Fig. 13. Schematic representation of the optical systems used for beam analysis of the Long Path laser.

of the Long Path laser. Our far-field camera uses a grating, constructed photographically, to produce multiple images whose relative intensities are controlled by the grating's characteristics. The several images provide data for a calibration curve of film density as a function of relative exposure. An important advantage of this system is its capability for self-calibration in a manner that eliminates concern over reciprocity failure.

The multiple film images produced by the far-field camera are scanned by a computer-operated microdensitometer that records the photographic density, as a function of position, on magnetic tape. We have written a computer program that converts the film density data and laser pulse characteristics to the following information, interpreted at the target: intensity contours, a three-dimensional intensity profile, the peak intensity, and the distribution of intensity and energy.

Figure 14 is an example of a three-dimensional intensity distribution and intensity contours for a firing of the Long Path laser.

Our technique for beam analysis will also be applicable to the new laser systems to be employed in future experiments. A more detailed description of the new method is in preparation.

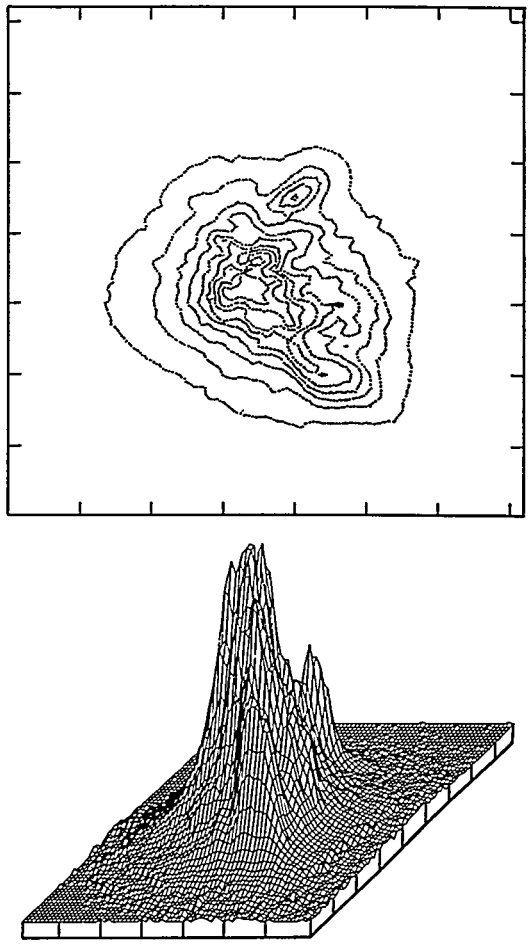

Fig. 14. Computer-generated reproductions of the far-field intensity profile of a Long Path laser pulse: contour plot above, three-dimensional representation below. The densities provided to the computer were from a multiple-image far-field photograph.

INSTRUMENTATION DEVELOPMENT

The activities of the Y-Division Diagnostics Group have proceeded in a variety of projects directed at the problem of obtaining high-resolution measurements of laser pulses and the characteristics of laser-produced plasmas. The capability of making detailed high-resolution measurements that provide characterization of the physical processes under study is essential to the progress of our program. Our development work on ultrafast streak cameras, applicable to a variety of wavelengths from the infrared to the x-ray region, has been very successful. We have begun investigating data-acquisition techniques for replacing

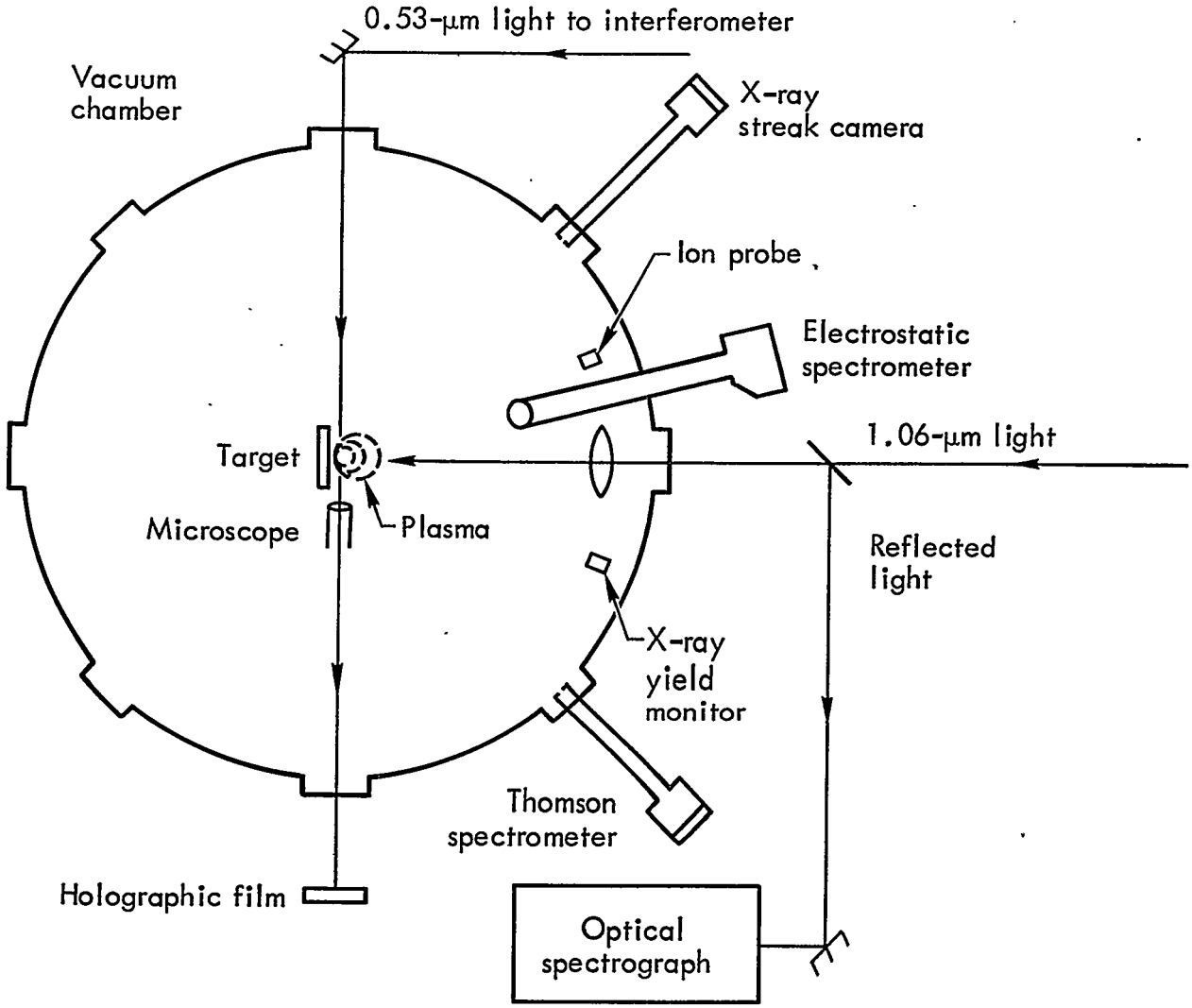

Fig. 15. Target chamber and some of the associated diagnostic equipment for studies of laser-induced plasma.

the film in the streak cameras. Techniques for diagnosing optical distortion in active lasing media have been worked out and the initial application to the study of the Nd:glass amplifier modules is imminent. Developments relevant to the target/plasma diagnostics have been in the areas of high-resolution interferometry and charged-particle diagnostics.

Diagnostics Laser-Plasma Laboratory

An important advance in our capabilities was provided by the operation of our Diagnostics Laser-Plasma Laboratory. A modest neodymium:glass laser produces nominally 1-J, 130-psec-FWHM pulses. We have used the output of this laser for testing and calibrating laser pulse diagnostics as well as for target irradiation in order to pursue the development of plasma diagnostics techniques. Figure 15 is a schematic diagram of the target chamber and some of the current instrumentation we are using; Fig. 16 is a photograph of the target chamber. We have irradiated slab targets of plastic and metal with focal spot diameters of about 200 μm. The results of work using

this facility are given in some of the following sections. The facility has provided an important and reliable tool for our diagnostics development.

X-Ray Streak Camera

The concept and the design modification of a standard image converter tube to make an ultrafast x-ray sensitive streak camera was mentioned in the previous annual progress report.[1] During the past year we have addressed the questions raised in that initial discussion. We have found that the sensitivity of our first rather crude camera is quite high, we have estimated the streak speed, and we have determined that the photocathode electron energy spread is not a severe limitation on time resolution for x rays in the few-kilovolt range.

The x-ray-sensitive streak tube was made by installing an x-ray sensitive photocathode and a new extraction grid into a standard, commercially available image converter streak tube (RCA C73435 series). The cathode is a 100-Å-thick gold layer supported on an 8-μm beryllium vacuum window.

In our initial experiments with the x-ray streak camera, shown schematically in Fig. 17, we placed a 0.3-mm-diam aperture in front of the x-ray photocathode. This aperture fixes the spatial resolution by limiting the usable photocathode area.

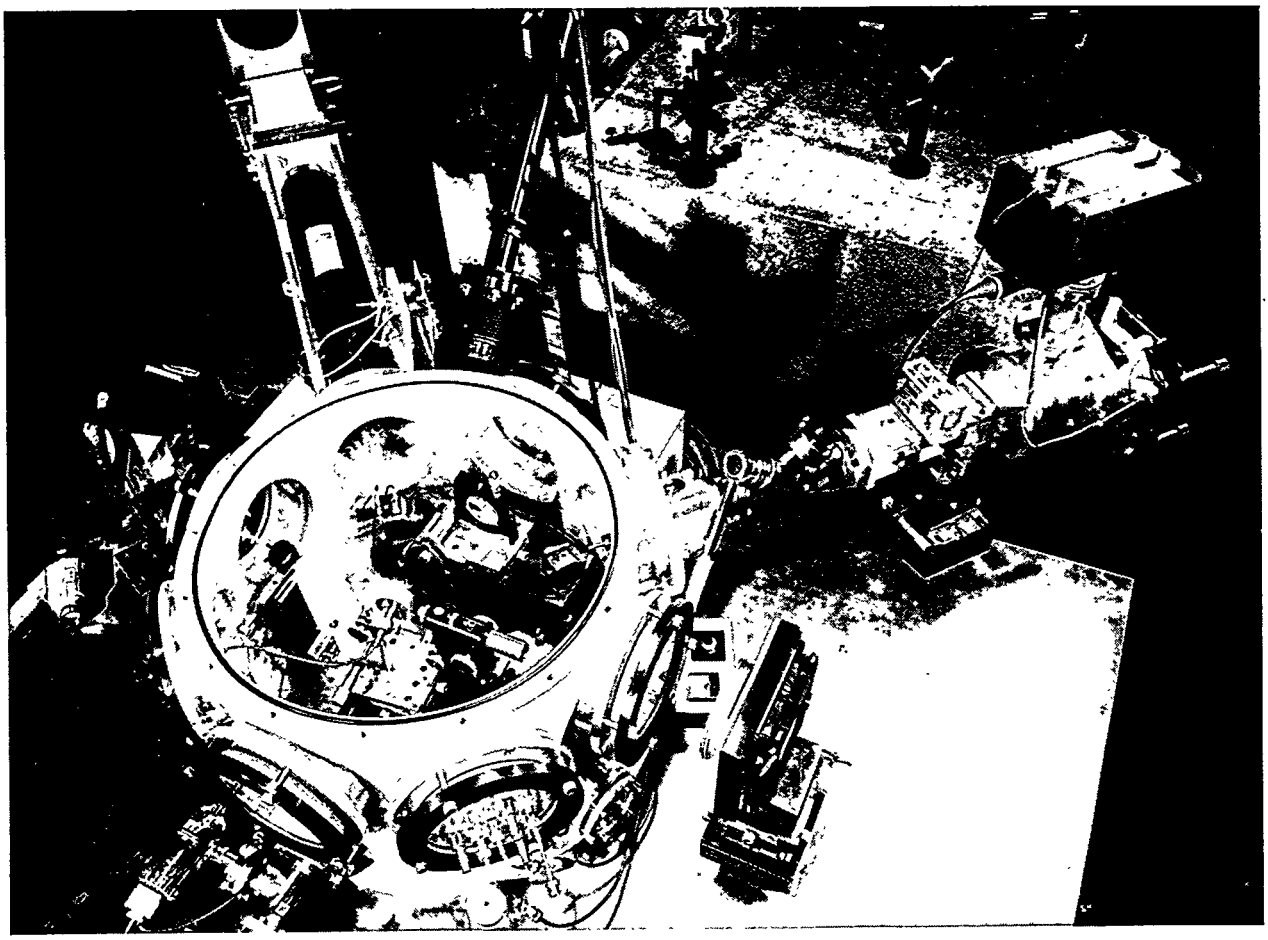

Fig. 16. Laser-plasma target chamber.

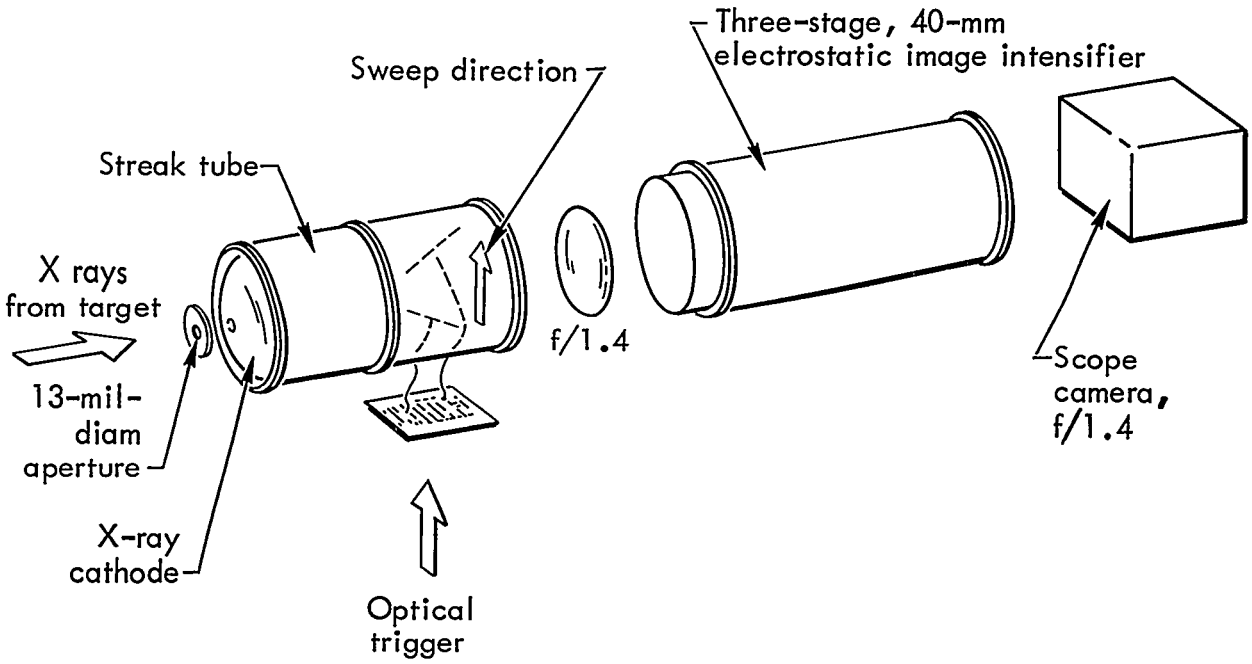

Fig. 17. Schematic diagram of our x-ray streak camera.

The resultant streak is a straight line of varying intensity. The camera shown in Fig. 18 uses components that were easily available. Because of the lens coupling and the characteristics of the image intensifier, the overall optical gain of the system is low – about 20. Nevertheless, the sensitivity of the camera is quite good. X-ray streaks have been obtained with the camera 10 in. from an iron target irradiated with a 1-J, 150-psec pulse from a Nd:glass laser. The exposure on the apertured cathode was on the order of 10 nJ of average 1-keV x rays.

We have determined the streak speed of the x-ray camera by observing the x-ray emission from an iron target during irradiation by two 0.5-J, 130-psec laser pulses separated by 300 psec. Figure 18 is a densitometer scan of the streaks with the streak photograph in the inset. The ripples in the densitometer scan are noise due to low incident flux and low film exposure. The resolution apparent in Fig. 18 is consistent with a time resolution of 50 psec.

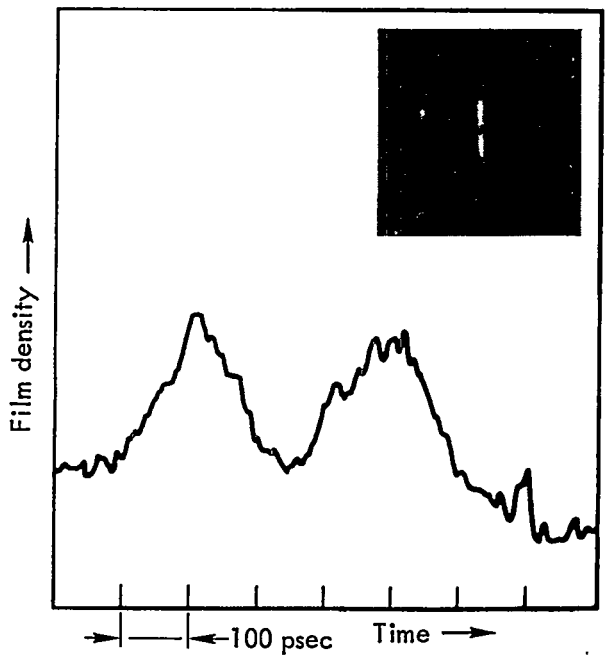

Fig. 18. Photograph obtained with the x-ray streak camera (top right) and its densitometer trace.

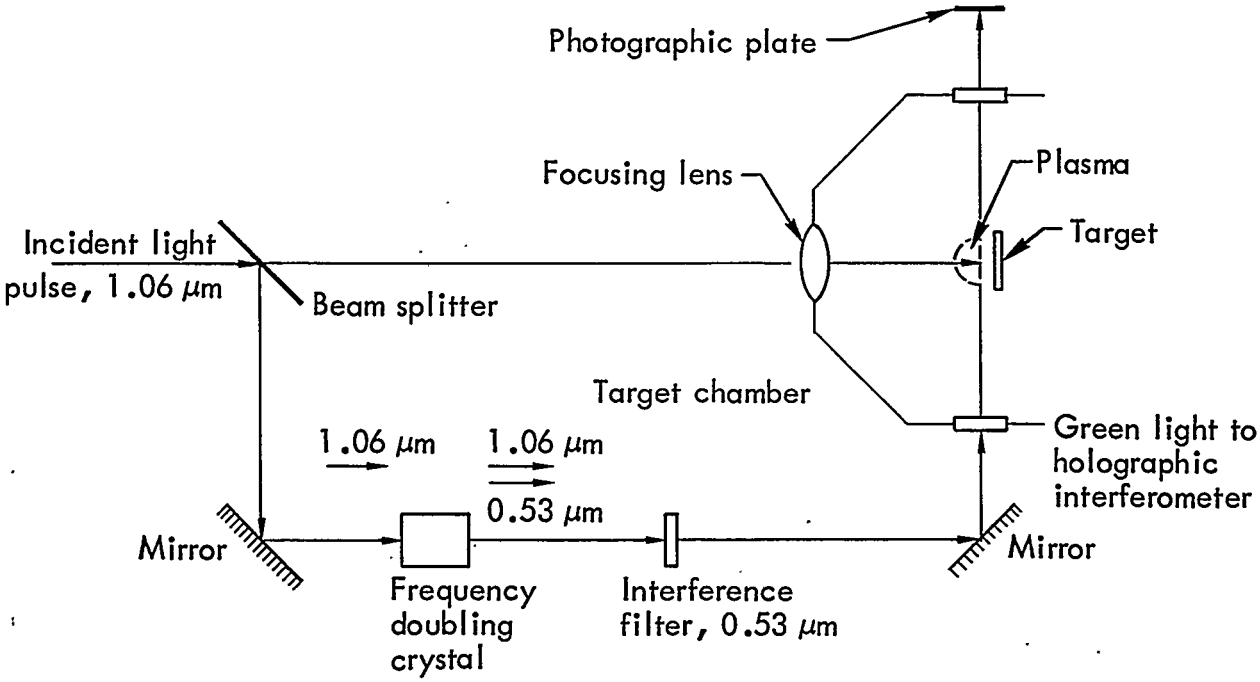

Fig. 19. LLL holographic interferometer experiment. A single laser is used both to produce and to diagnose the plasma.

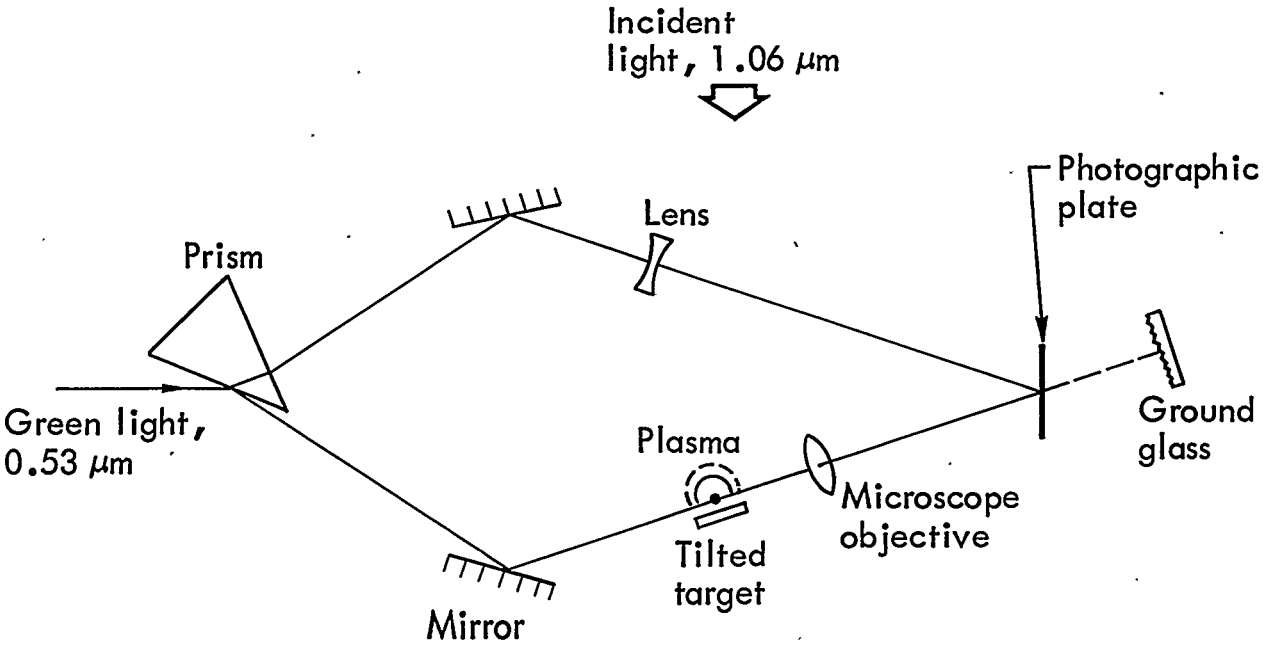

Fig. 20. Optical interferometer used in the holographic experiment illustrated in Fig. 19. The interferometer uses holographic microscopy.

We are now building a new x-ray streak camera with a 1 cm by 125 μm slit photocathode. The tube has a fiber-optic output window and will be contact-coupled to a high-grain microchannel-plate image intensifier as used in optical streak cameras. This will provide higher light gain and better usable range on the recording film. The slit cathode on new camera will provide 1° of spatial resolution, making possible time-resolved measurements of x-ray spectra and spatial-intensity (imaging) variations that will substantially enhance our diagnostics capabilities for laser-produced plasmas, which in turn will provide fundamental information necessary for effective target design.

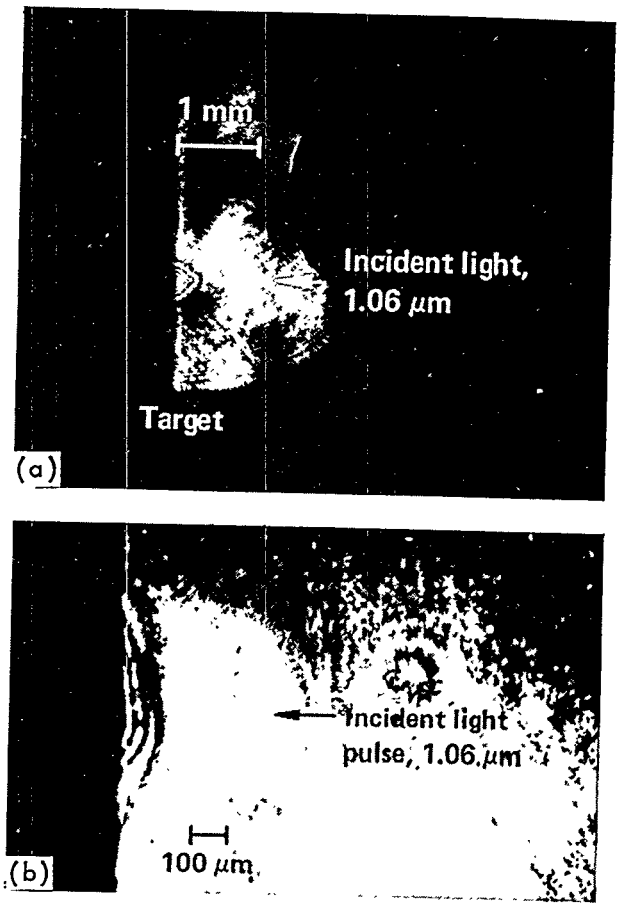

Fig. 21. Interferograms of laser-produced plasmas obtained using holographic microscopy: (a) delay time 1 nsec after irradiation, (b) delay time 0.5 nsec after irradiation.

Holographic Microinterferometry of Laser Produced Plasmas

During the past six months we have extended the use of a holographic scheme to obtain microinterferograms of laser-produced plasmas with a temporal resolution of approximately 100 psec. A single laser is used for both production and diagnostics of the plasma, as shown in Fig. 19. A sample of the main heating pulse is split off and frequency doubled at 5320 Å before entering the interferometer. The holographic interferometer is shown in Fig. 20. The only unusual element is the microscope objective, which permits us to obtain high spatial resolution. The absence of diffuse surfaces between the laser and holographic plate eliminates the diffractive effects of coherent speckle. Figure 21 shows two results obtained with this technique; each was obtained with 0.5 J of 1.06-μm radiation focused to a 200-μm spot on the surface of an aluminum slab. The duration of the heating pulse was approximately 150 psec FWHM. In the interferogram obtained at a delay time of 1 nsec after the arrival of the 1.06-μm heating pulse, six fringes are evident, indicating an electron density of $10^{20}/cm^3$ 40 μm from the slab surface. The spatial resolution evident here is approximately 30 μm, a value determined by the 0.1 nsec duration of the diagnostic pulse and the observed fringe velocity of 300 μm/nsec. The interferogram obtained at a 0.5-nsec delay shows three fringes. In this case, the main laser pulse was not focused on

the surface of the target; hence the flattened appearance.

Future work will concentrate on development of shorter diagnostic pulses, which will improve spatial resolution, and the use of shorter-wavelength probing radiation. The use of 3547-Å or 2660-Å radiation will reduce refractive effects within the plasma and reduce the number of fringes in higher-energy laser systems. The ultimate goal of this program is to determine the spatial distribution of electron density in the vicinity of the critical (10^{21} electrons/cm^3) surface associated with the heating of 1.06-μm pulse. The determination of density gradients in this vicinity will aid in determining the importance of competing absorption and reflection processes in laser-produced plasmas.

Ion Spectroscopy of Laser-Produced Plasmas

We have built two diagnostic devices for the ion spectroscopy of laser-produced plasmas. We have constructed a 127° curved-plate electrostatic energy analyzer and a Thomson mass spectrometer from basic designs provided by Sandia Laboratories, Albuquerque. Both devices have been used to observe plasmas produced by subnanosecond, 1.06-μm laser pulses striking planar targets in our diagnostics facility.

We have used the curved-plate electrostatic energy analyzer, shown in Fig. 22, to measure the energy and charge distributions of ions emanating from laser-produced plasmas. This is basically a time-of-flight device in which only ions of a preselected energy-to-charge ratio pass through the spectrometer and reach the detector at times determined by the masses of the ions and their kinetic energies. Figure 23 shows a representative analyzer output. This device requires many repeatable laser firings to determine average energy and charge distributions of the ions; however, it is

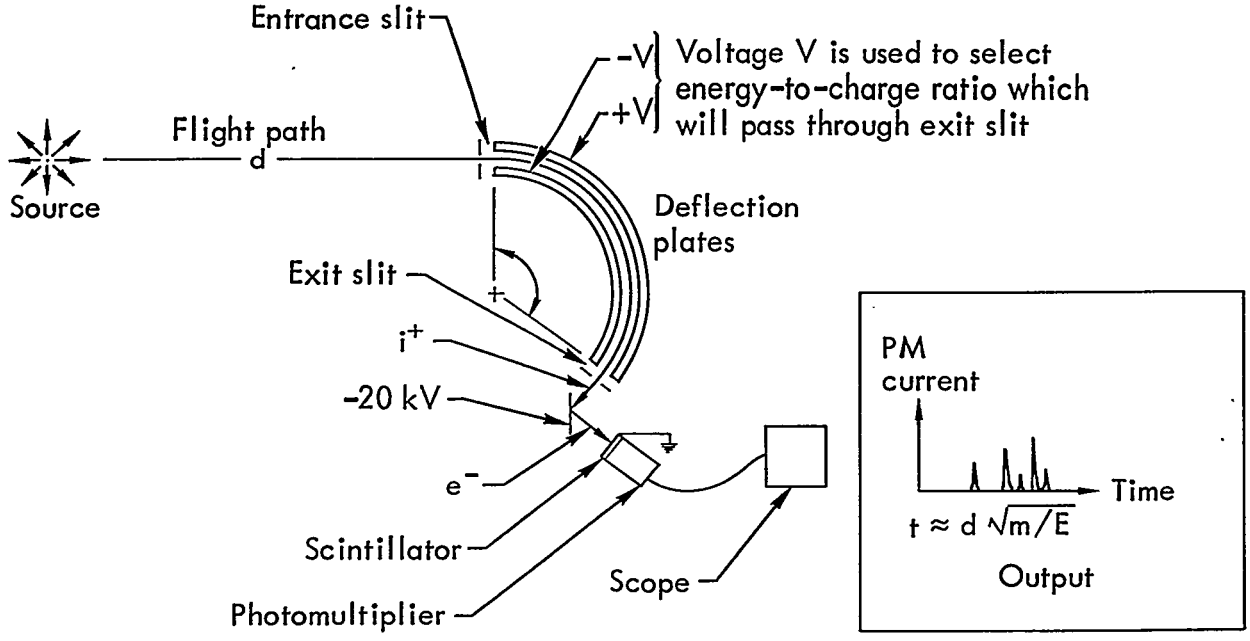

Fig. 22. Curved-plate electrostatic energy analyzer for ion spectroscopy of laser-produced plasmas.

well suited for studies at particular energies.

The Thomson spectrometer, (Fig. 19 of Ref. 1) is capable of measuring a wide range of ion energy and charge distributions on one shot. It uses parallel magnetic and electric fields to spatially separate ions of different energies and charge-to-mass ratios. Ions with the same charge-to-mass ratio form a parabola at the output; position along with the parabola is directly related to ion energy. A separate parabola is obtained for each individual ion species, so that the output appears photographically as a series of parabolas. The density of the photograph at any point on a parabola is related to the number of ions of that charge to mass ratio with that energy. A novel feature of this instrument is the use of a channel-electron-multiplier

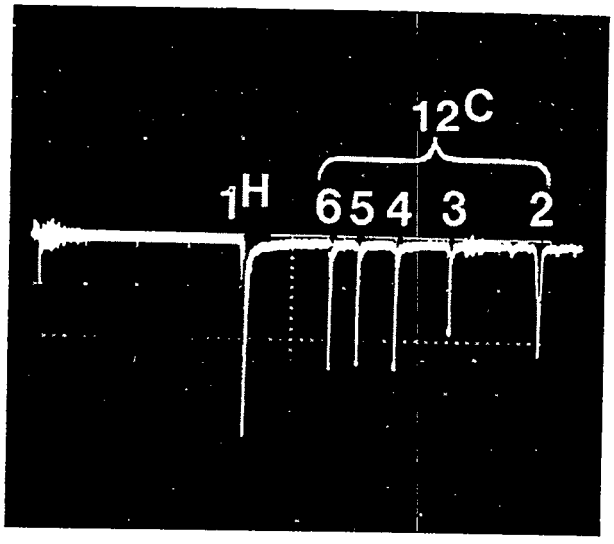

Fig. 23. Typical output of the curved-plate energy analyzer, showing the ion currents from a CH_2 target. The peaks are due to $^{1}H^{+}$ (1.05 keV), $^{12}C^{2+}$ (2.10 keV), $^{12}C^{3+}$ (3.15 keV), $^{12}C^{4+}$ (4.20 keV), $^{12}C^{5+}$ (5.25 keV), and $^{12}C^{6+}$ (6.30 keV). The scope sensitivities are 0.5 V/division and 1 μsec/division.

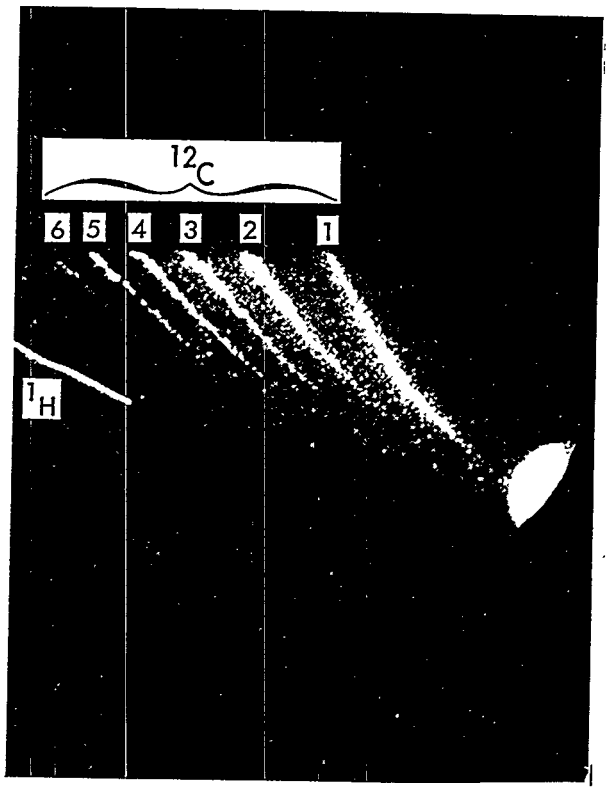

Fig. 24. Photo taken with the Thomson spectrometer after irradiation of a CH_2 target. All six carbon species are shown.

array to amplify the signal while retaining spatial information; this array converts ions to electrons, increases the number of electrons by secondary emission along a continuous dynode, and finally accelerates the electrons to a phosphor-coated screen that can be photographed. Figure 24 is a photograph taken with the instrument after irradiation of a CH_2 target. The parabolas corresponding to ionized hydrogen and all six carbon species are clearly visible.

X-Ray Detector Array

We are presently developing a high-quality seven-channel x-ray detector array for use in the 1-15 keV energy range. The silicon detector outputs will

be integrated and sequentially read for display on an oscilloscope or eventually interfaced to a computer. This small array will allow coarse spectral surveys in this energy range to be observed on a routine basis with a minimum commitment of equipment and minimum target-chamber access.

Future Work and Projected Activities

In the past, progress toward our goal of building an efficient x-ray simulator has been limited by the availability of (1) high-quality, well-characterized, short-pulse, high-power lasers; (2) targets with characteristics determined by LASNEX calculations to be capable of efficient conversion of laser energy into x-ray radiation; and (3) diagnostics with high spatial (~1-10 μm) and temporal (~10 psec) resolution capable of providing detailed information about the x-ray radiation field. To overcome these difficulties and make further progress toward the development of an intense x-ray source, we have developed two new, high-quality, well-characterized short-pulse, high-power laser systems: Nd:YAG-glass laser system and a CO_2 gas laser system. In addition, extensive diagnostics development and target fabrication programs are in progress.

The Nd:YAG-glass laser is a two-beam laser system capable of producing 50-J/beam output pulses of 0.1 to 1 nsec duration at 1.06 μm wavelength. The CO_2 laser system is capable of producing 50-J output pulses of 1 to 2 nsec duration at 10.6 μm wavelength. Single-beam irradiation experiments will begin in July 1974. Shortly thereafter a second beam will be available on the Nd:YAG-glass laser system for two-sided irradiation experiments and also for producing short x-ray pulses for plasma diagnostics purposes.

Experiments with these two laser systems will be performed with equivalent targets and diagnostics so as to provide detailed information concerning the laser wavelength scaling laws for the conversion of laser energy to x-ray energy. Of particular interest is the dependence of the x-ray total energy yield, the x-ray emission efficiency, and the x-ray emission spectrum on the wavelength of the incident laser radiation for comparable laser pulse and target conditions. We will use the diagnostics described earlier in this report to provide sufficient information to compare LASNEX computer calculations with experimental results. We will use these comparisons to upgrade the LASNEX computational model and to design more efficient laser-to-x-ray-energy conversion targets.

The comparison of available diagnostic techniques and the development of new ones will continue to be an important part of the program. We will emphasize the development of diagnostics with better spatial and temporal resolution, such as the 50-psec x-ray streak camera and a more sensitive x-ray microscope. We will explore alternatives to the present x-ray emission spectrum diagnostics. Efforts to synchronize a short pulse (<20 psec) laser with the Nd:YAG-glass

and CO_2 irradiation lasers will receive increased support, because the mastery of this technique will provide the capability to make microscopic holographic interferograms and framing pictures of the plasma development during irradiation. We are also actively investigating the feasibility of interferometry with ultraviolet and soft x-ray radiation. Also under consideration are techniques to measure the total radiation field and plasma particle energy balance. These diagnostics will provide information about the efficiency of the laser-plasma coupling.

We need to ascertain whether the LLL laser program will be able to satisfy DNA requirements on x-ray fluence and spectral distribution. LASNEX calculations predict that the 10-kJ, 100-psec Nd:glass laser to be completed in 1977 will be suitable for producing intense x radiation. Figure 25 gives the calculated x-ray spectrum produced in the irradiation of a thin spherical lead shell with this laser. Both calculations assume hydrogenic average atom opacities; one assumes LTE, the other non-LTE. Both predict a mean photon energy of 4-5 keV; the LTE calculation predicts a total x-ray fluence of 6 kJ, the non-LTE calculation 4 kJ.

JANUS, A TWO-ARM Nd:GLASS SYSTEM

Janus Laser

We are now assembling an improved Nd:glass laser system to replace the Long Path laser for target-irradiation studies. Figure 26 is an artist's concept of the completed laser. This laser will provide two opposing beams on the target and will be used for both single-beam and two-beam experiments. System output power capability will be up to 5×10^{11} W per beam in a well-characterized light pulse. The system built from replicas of laser components that were designed for the planned Livermore High Energy Laser Facility and are now undergoing development testing in our Cyclops laser system.[6]

Pulses for amplification in the laser are produced in a mode-locked Nd:YAG oscillator with single-pulse switchout. This oscillator has been engineered to provide reliable and reproducible operation under conditions normally encountered in the laboratory.[7] The output pulse energy is about 2 mJ and the pulse duration may be tuned from 30 psec to about

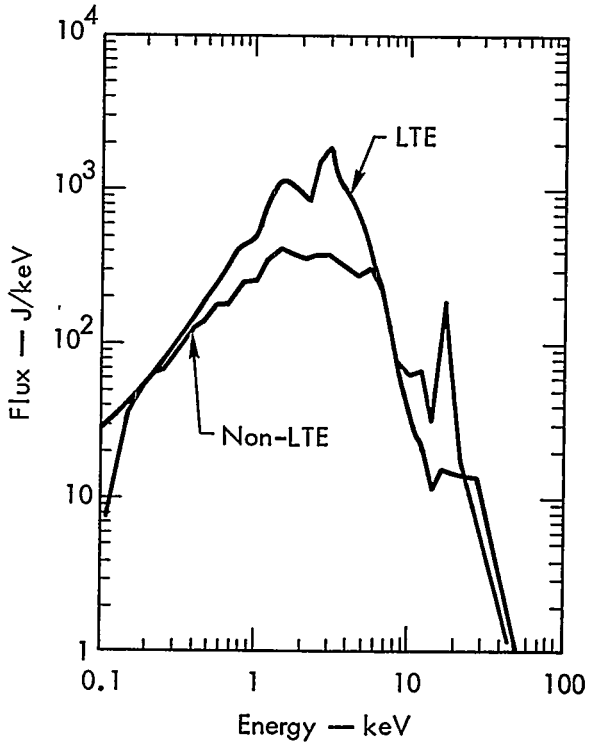

Fig. 25. X-ray spectra predicted by LTE and non-LTE calculations of the irradiation of a 100-μm-diam, 4-μm-thick lead shell by the 10-kJ, 100-psec laser.

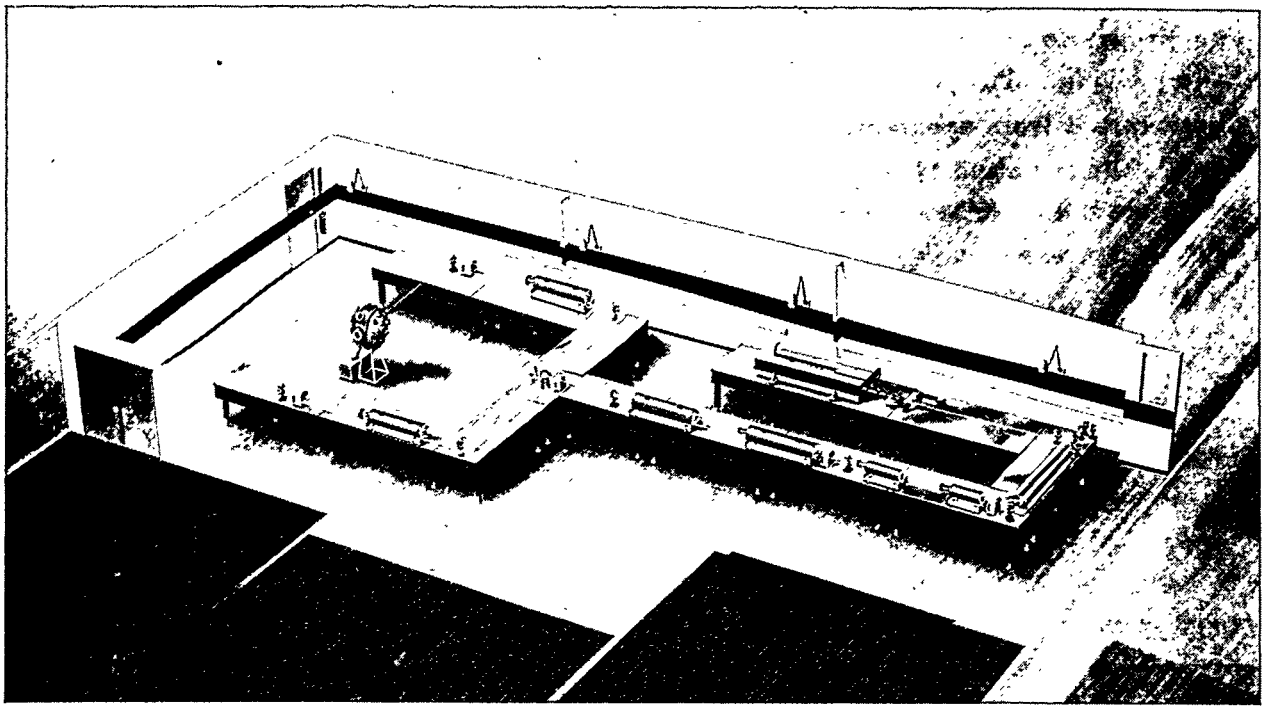

Fig. 26. Artist's concept of the two-arm (Janus) laser system for target-irradiation studies.

1 nsec. Longer pulses will be available from an alternate oscillator now in design and construction.[8] Limited pulse shaping will be available by dividing and recombining the pulses after it has left the oscillator. We are initially setting up the laser with pulses of about 150 psec duration.

The amplifier train will consist of a Nd:YAG preamplifier, a glass-rod preamplifier system and a series of glass-disk amplifiers of 3.5 and 8.5 cm aperture. The glass rod preamplifier contains three 2.5-cm-diam by 25-cm-long glass rods and two Faraday isolators in a single chassis. Each of the glass rods produces a nominal gain of ten. The disk amplifiers each contain six elliptical glass disks and have a nominal gain of 3.5. Total system gain after losses are taken into account is approximately 10^5.

The system output is limited by damage and beam distortion caused by self-focusing and is expected to be 50 J per beam for a 100 psec pulse. Output energy is maximized by amplifying a temporally and spatially smooth pulse. The temporally smooth pulse is generated in the oscillator. The spatially smooth beam is produced by a spatial filter at the output of the oscillator and an apodized aperture at the input to the rod amplifier, which produces an optimum beam shape for propagation through the amplifier train. The beam is of uniform intensity over most of the aperture but truncates smoothly enough that it will propagate through the amplifier train free of diffraction fringes. Diffraction fringes are undesirable because they create small-scale intensity fluctuations that self-focus and cause damage to the laser components.

Pulsed Faraday rotators and polarizers[9] at appropriate locations in the amplifier train provide isolation from target reflections and from spontaneous oscillations. The isolation system is designed to protect the laser from damage even if 100% of the laser energy returned from the target.

We have designed and built a target chamber (also shown in Fig. 26). The chamber has 26 ports providing two ports for the focusing lenses, one port (on top) for a target positioner, one port for vacuum pumpout, and three ports for target-positioning optics. The remaining ports are for plasma diagnostic measurements, which will include a variety of optical, charged-particle, x-ray, and other measurements.

Assembly of the system is in progress. The planned x-ray diagnostics include x-ray microscopy, bent-crystal spectroscopy, K-edge-filter spectroscopy, and x-ray calorimetry. The schedule is presently determined by the delivery of glass disks and flashlamps; operation with a single beam on target with about 5 J hopefully can begin in early FY 1975, with full two-beam operation following about a month later.

Janus Target Chamber

The target chamber is fabricated from a 24-in.-diam stainless steel cylinder and two elliptical ASME heads (Fig. 27).

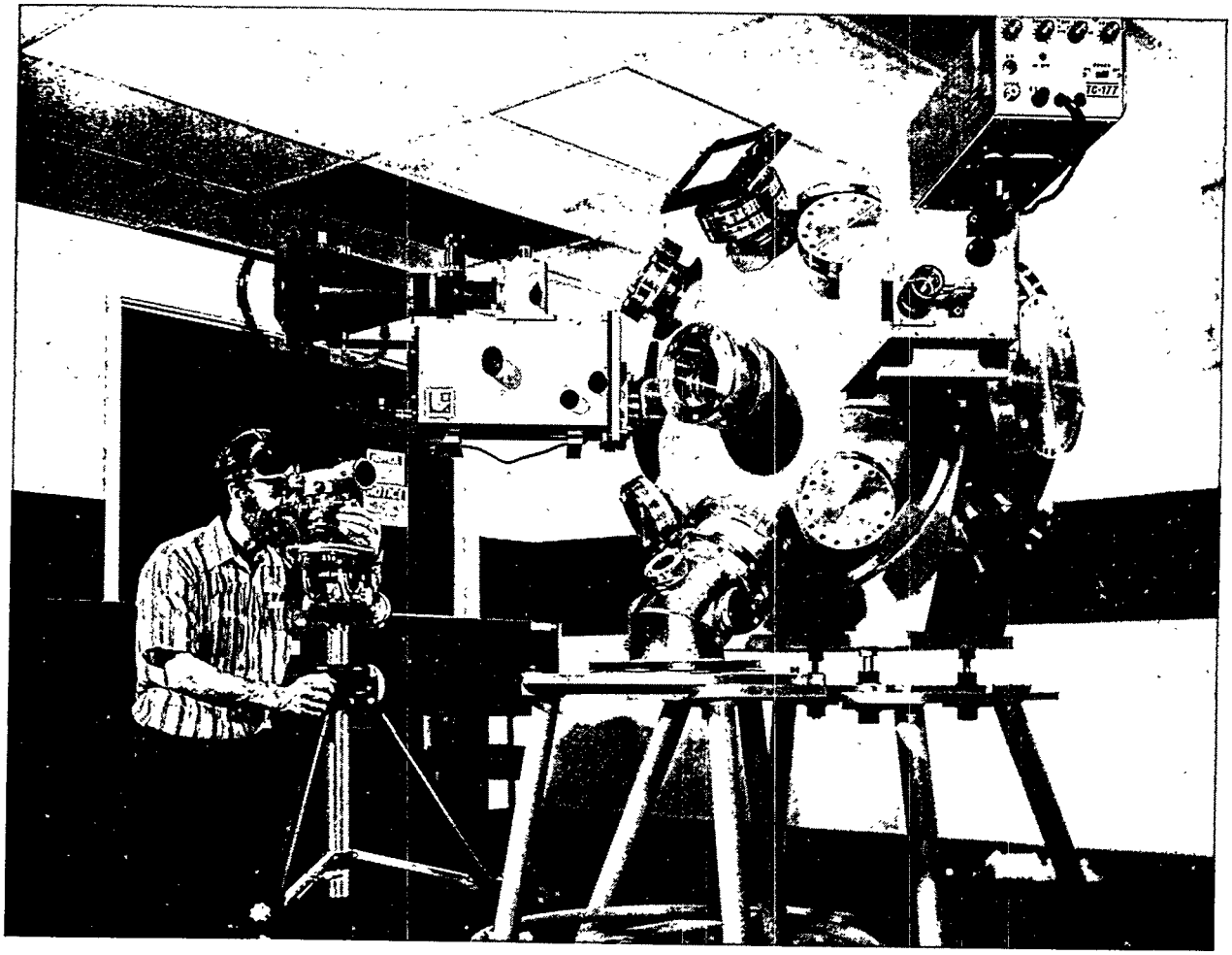

Fig. 27. Target chamber for the Janus laser system.

Ports are provided for two opposing laser beams, a target holder, three target-alignment optical systems, and a vacuum line. Nineteen ports of 4 and 6 in. diameter are provided for beam and target diagnostics. One head is removable for ease of access when installing large components inside the chamber. The base is adjustable in all axes for accurate positioning and leveling.

The vacuum system consists of a mechanical roughing pump, a 500 liter/sec Temescal turbomolecular pump and a 6-in. Temescal cryogenic pump, all sized for a planned base pressure of 10^{-6} Torr. Controls are completely automatic and fail-safe. An additional mechanical pump is available for roughing auxiliary equipment as needed.

The incoming beam intensity is proportional to $\exp -(r/r_a)^{10}$ where r_a is 28.5 mm. The lenses have a clear aperture of 85 mm, corresponding to 10^{-3} times the maximum intensity. Both f/1 and f/2 aspheric lenses have been ordered. Lens position is adjusted in x, y, and z coordinates by Aerotech motorized translation stages and in ϕ and tilts by LLL-designed stepping-motor drives. All motorized drives operate in the chamber vacuum.

Target positioning is done using a manually operated Varian manipulator (Fig. 28). Position is verified using specially made alignment optics, which are also used to view the target during the experiment using hard film, infrared TV cameras, or high-speed streaking cameras.

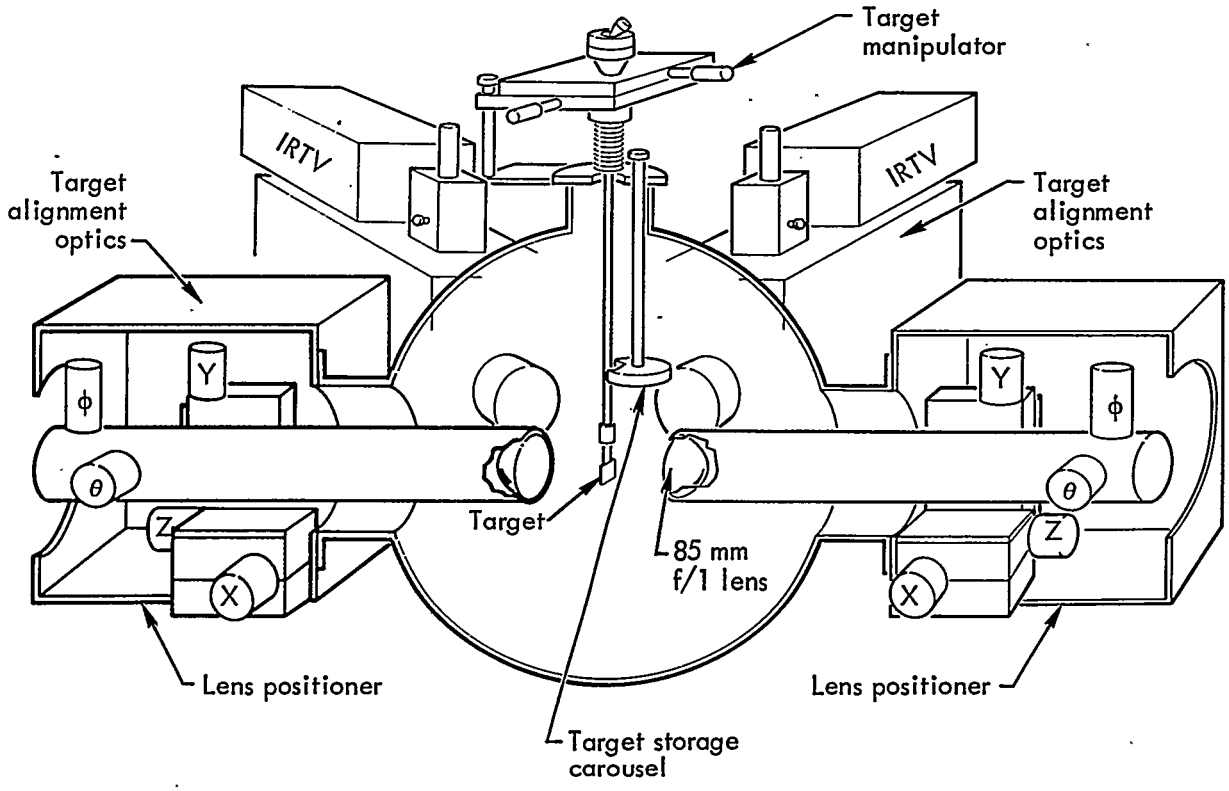

Fig. 28. Target-positioning, target-alignment, and lens-positioning systems for the Janus laser.

[redacted]

The target-alignment optics system (Fig. 28) uses a relay lens to focus a full-size image of the target on an adjustable reticle that is contained in the system. The reticle and the target image are then viewed with standard microscopy optics. Movable mirrors allow this image to be viewed visually or transferred to a photographic recording system.

The target-alignment optics systems are aligned by first introducing a spherical reflecting target into the focused CW YAG beams and aligning it by considering it to be the reference sphere in a shear-plate interferometer configuration. After the ball is aligned in a YAG beam, the alignment optics are adjusted to center on the sphere. The sphere is then replaced by a target that is moved until it is centered on at least two orthogonal alignment systems.

Provision is made for exposing a number of targets in sequence without destroying the vacuum. Up to 12 targets are stored in a carousel in special magnetic holders. The end of the Varian manipulator is provided with a switchable magnet to allow picking up a new target or releasing a spent target to the storage carousel.

CO_2 LASER SYSTEM

The objectives of the CO_2 laser system have been to construct an intermediate-size CO_2 laser system for examining system scaling laws and performing plasma physics experiments.[10] Because our laser system was dedicated from its inception as a facility for target interaction studies, we have imposed several requirements on its design: (1) reliability must be high; (2) the pulse repetition rate should be at least one pulse per minute, so that data can be acquired in a reasonable time span; (3) preventive maintenance to ensure reliability should not be required more often than every 1000 shots; and (4) electrical noise must be minimized within reasonable economic limits.

CO_2 Laser

The CO_2 laser system consists of devices that we rigidly specified and then purchased from vendors who normally sell similar units. Following our mode-locked TEA oscillator and Ga-As $\lambda/2$ switchout unit, we have assembled an amplifier chain consisting of a uv-preionized TEA preamplifier, a beam expander with a magnification of three, and a 9-cm-aperture uv-preionized TEA amplifier, following by two 11-cm-aperture cold-cathode electron-beam-sustained amplifiers operated at 2 atm. Our system is designed to produce spatially smooth 1.5-nsec-duration 10.6-μm pulses containing about 50 J. It should be possible to extract more than 50 J, but only at the expense of beam quality.

During the past six months our experimental studies have continued to provide improved input for computer programs designed to simulate the energy extraction efficiency and pulse shapes from the high-power CO_2 lasers being assembled for laser-fusion experiments. Generally these experimental and theoretical findings have supported our confidence in the validity of our initial design, and, consequently, the largest part of our effort has been directed toward the realization of this system.

[redacted]

Fabrication of the CO_2 laser system is on schedule; we expect the system to be fully operational in early FY 1975. Figure 29 shows the CO_2 laser system and target chamber. The oscillator system and first large-aperture amplifier are operational and characterized, and the two electron-beam-sustained amplifiers are installed and under test. The facilities are essentially complete; the control and diagnostics instrumentation are in the final phase of completion.

This CO_2 laser facility will make possible vital plasma physics experiments for examining the properties of the light-plasma coupling. By using visible-wavelength pulsed holographic and interferometic techniques, we can study in detail the heating of a target plasma by a 10.6-μm pulse. Such information is necessary for the testing and normalization of computer models for laser heating of high-density target plasma. Early experimental studies using the CO_2 laser system will be attempts to elucidate this light-plasma coupling phenomenon.

CO_2 Target Chamber

The target chamber (Fig. 30) is a 26-ported high-vacuum chamber providing a 27.8-in.-diam central spherical zone free of any obstructions. The chamber is separable into two major parts by disassembly of a midsection separation

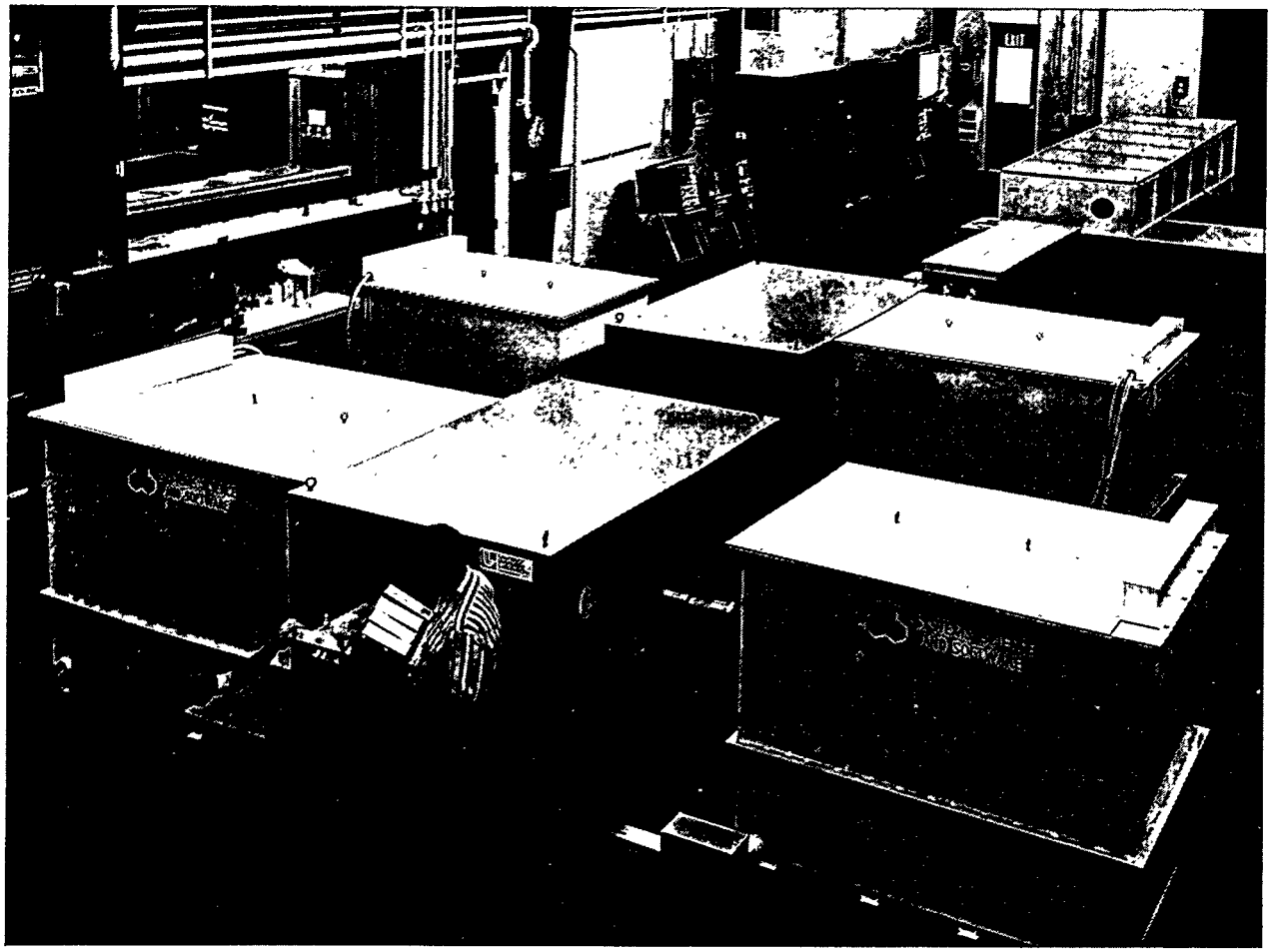

Fig. 29. Artist's concept of the CO_2 laser system and target chamber.

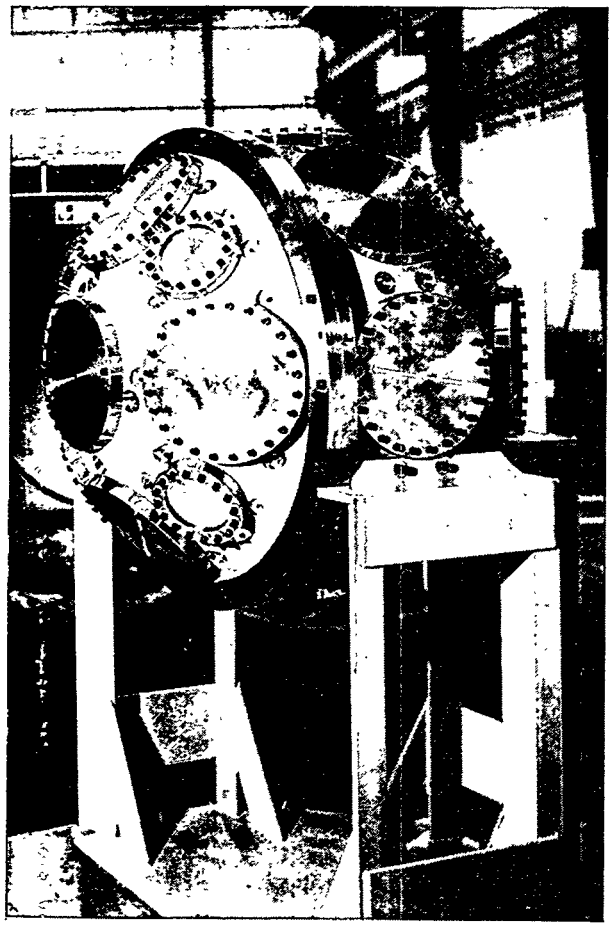

Fig. 30. Target chamber for the CO_2 laser system.

flange pair using an O-ring seal. The separation plane is just south of the equatorial ports. The port flange planes are normal to the chamber radius. All 26 ports have a Varian high-vacuum sealing knife edge machined into the chamber so that the chamber can be fitted with standard Varian flanges. Three or four drilled and tapped equipment mounting spots are provided around each port. The vacuum system consists of a 500-liter/sec turbomolecular pump in conjunction with a cryopump and backed by a cryotrapped 17.7-cfm forepump.

Target positioning is done with a five-axis positioner, which picks up targets out of a supply retained in a carousel that also can be moved. The target is aligned by two orthogonal microscopes.

X-RAY MEASUREMENTS

X-ray spectra measurements for upcoming laser beam targets will require radically different diagnostics from those previously used with the Long Path laser. Of particular interest will be the very high fluxes anticipated from the microdot x-ray converter targets. Figure 31 compares the measured spectrum from a carbon target used with the Long Path laser and the calculated spectrum from a lead microdot target. For most energies shown in this graph, orders of magnitude separate the two spectra. We are now building instrumentation to measure this high-intensity microdot spectrum. The importance of developing these diagnostics to measure this spectrum is underscored by the fact that the whole purpose of this effort is to convert laser energy to x-ray energy. Table 4 shows the instrumentation being developed and the x-ray energy range each instrument covers. Each instrument is briefly described below.

UV Spectrometer – We are building a lead stearate curved-crystal spectrometer for making measurements between 0.25 and 1.1 keV. The data will initially be recorded on film; eventually we will have an active readout using MOSFET detectors.

Bent-Crystal Spectrometer – We are building a KAP curved-crystal spectrometer to cover the energy range from 0.5 to 7 keV. This will be a high-resolution

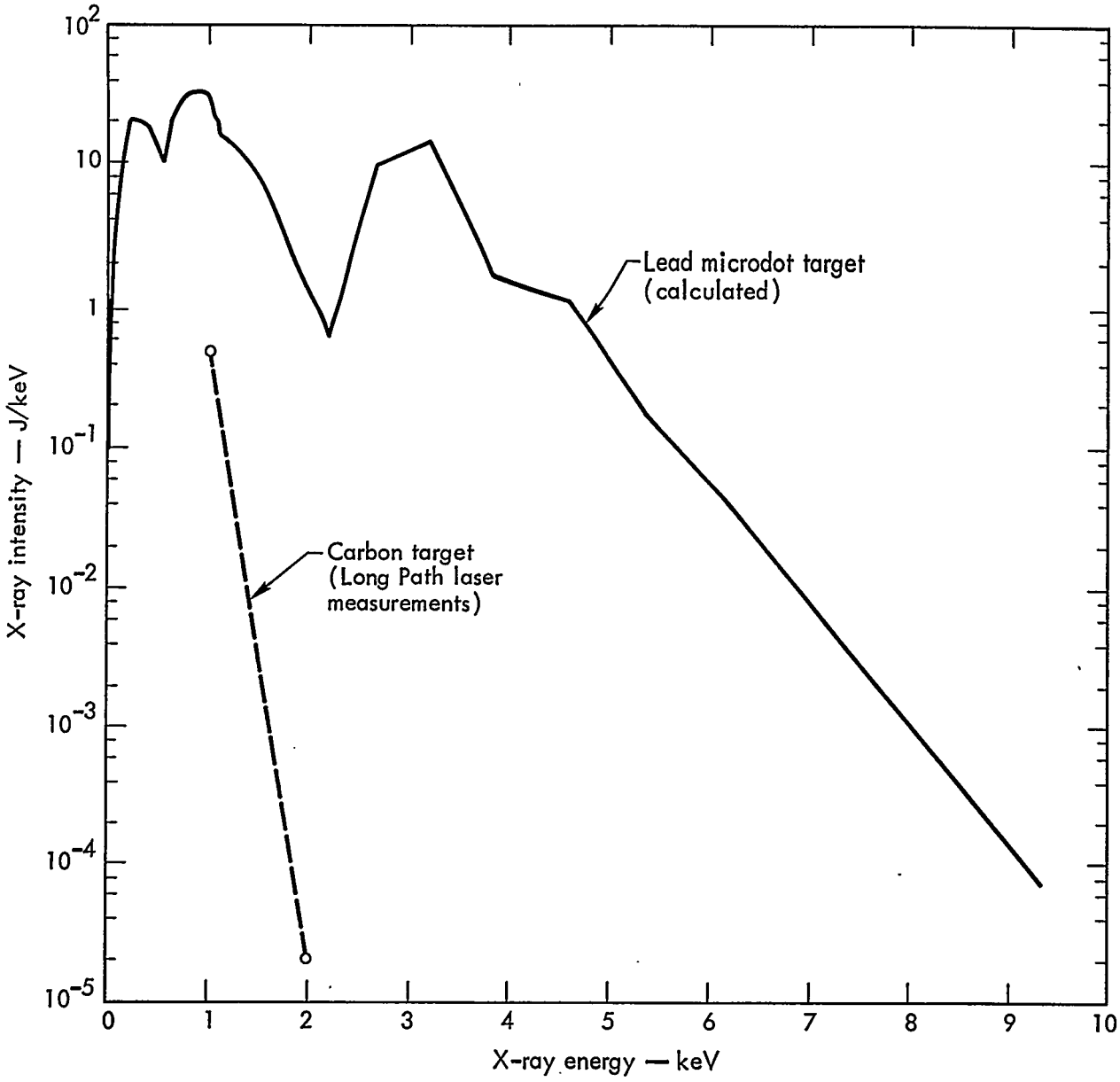

Fig. 31. Comparison of calculated and measured x-ray spectra.

instrument (<1 eV at 1 keV) using film to record the data. Solid-state PIN detectors will also be used in the film plane to record data. The active readout mode will not be high resolution.

X-Ray Diode Array – To directly measure the low-energy x rays we are building a new type of x-ray detector using the photoelectric detector principle. This detector is essentially a stack of

Table 4. X-ray diagnostic instrumentation under development.

Instrument	Energy range (keV)
UV spectrometer	0.25 - 1.1
Bent-crystal spectrometer	0.5 - 7
X-ray diode array	1.5 - 6
Silicon diode array	6 - 50
Photomultiplier array	6 - 100

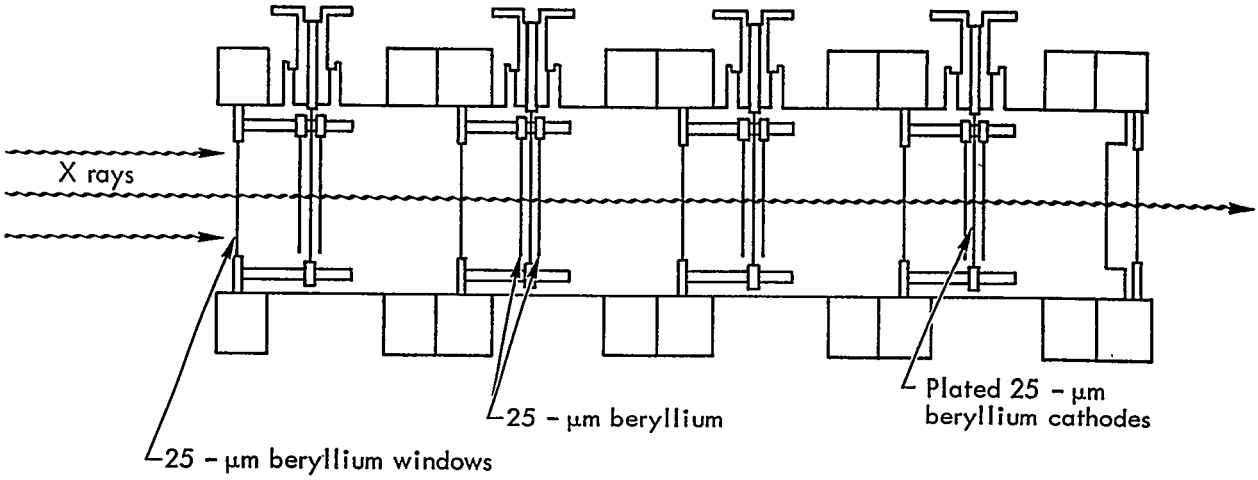

Fig. 32. Sketch of x-ray diode array. The cathode of the first detector (far left) is plated with aluminum; this detector measures 1.5 keV x rays. Succeeding cathode plating materials and x-ray energies are aluminum, 3 keV; gold, 4.5 keV; and chromium, 6 keV.

four x-ray detectors to measure four discrete x-ray energies on one vacuum-chamber port. Figure 32 is a sketch of this stack.

The insensivity of these detectors allows them to be put directly in the x-ray beam without the flux being reduced by diffraction. Energy discrimination is accomplished by putting K-edge filters in front of the cathodes and using the combination of filter transmission and photocathode absorption to effect a "band-pass." A superb feature of the detector is that it can be calibrated absolutely using our x-ray facilities.

Silicon Diode Array — We have extensive experience at LLL using silicon PIN diodes as calorimeters to measure low-energy (about 1 keV) x rays. We are extending the range of the detectors and constructing a K-edge filter spectrometer using an array of seven PIN diodes to measure the microdot x-ray spectrum from 6 to 50 keV.

Photomultiplier Array — The photomultiplier array with K-edge filters is essentially the same as described earlier in this report (p. 26). This system was developed and used successfully by LLL to measure the high-energy x rays from a carbon target. This array can be used to measure the high-energy x rays from microdot targets.

We are also proceeding with the development of high-intensity monoenergetic x-ray sources in the 0.1-100-keV energy range for detector calibrations. It is anticipated that all of the final spectrum measurements will be absolute so that the measured laser-energy-to-x-ray-energy conversion efficiencies can be compared absolutely with code predictions.

Currently under construction is a computer system to handle the plethora of data expected from the diagnostics. The ultimate aim of the computer system is to digitize the data when possible and have a direct link to the LLL Computation Center for rapid analysis of the data.

[redacted]

References

1. S. W. Mead, Ed., X-Ray Emission from Laser-Produced Plasmas, Lawrence Livermore Laboratory Rept. UCRL-51421 (1973) (title U, report SRD).
2. P. J. Mallozzi, H. M. Epstein, R. G. Jung, D. C. Applebaum, B. F. Fairand, and W. J. Gallagher, Final Report on X-ray Emission from Laser Generated Plasmas to ARPA, Battelle Memorial Institute, Columbus, Ohio, 1972, Vol. II.
3. D. J. Nagle, Naval Research Laboratory, Washington, D.C., private communication.
4. L. F. Chase, Lockheed Palo Alto Research Laboratory, Palo Alto, Calif., private communication.
5. Laser Fusion Program: Semiannual Report – January-June 1973, Lawrence Livermore Laboratory Rept. UCRL-50021-73-1 (1973), pp. 171-174.
6. Ibid., pp. 4-5.
7. Ibid., pp. 31-33.
8. Ibid., pp. 33-36.
9. Ibid., pp. 78-82.
10. Ibid., pp. 116-129.

[redacted]

[redacted]

Distribution

Series A

	Copy No.
LLL Internal Distribution	1-75
External Distribution	
RARP (G. K. Soper) Defense Nuclear Agency Washington, D. C.	76-77
M-3679 Distribution, C-74 Nuclear Weapons Related Engineering, Instrumentation and Materials	78-94

RCB/lc/edas

[redacted]